


ORIGINAL RESEARCH

Estrogen Plays a Crucial Role in Rab9-Dependent Mitochondrial Autophagy, Delaying Arterial Senescence

Yuichi Sasaki, MD, PhD; Yoshiyuki Ikeda , MD, PhD; Yoshihiro Uchikado, MD; Yuichi Akasaki, MD, PhD; Junichi Sadoshima, MD, PhD; Mitsuru Ohishi, MD, PhD

BACKGROUND: The risk of cardiovascular disease is known to increase after menopause. Mitochondria, which undergo quality control via mitochondrial autophagy, play a crucial role in the regulation of cellular senescence. The aim of this study was to investigate whether the effect of estrogen-mediated protection from senescence on arteries is attributed to the induction of mitochondrial autophagy.

METHODS AND RESULTS: We used human umbilical vein cells, vascular smooth muscle cells, and 12-week-old female C57BL/6 mice. The administration of 17 β -estradiol (E2) to cells inhibited cellular senescence and mitochondrial dysfunction. Furthermore, E2 increased mitochondrial autophagy, maintaining mitochondrial function, and retarding cellular senescence. Of note, E2 did not modulate LC3 (light chain 3), and ATG7 (autophagy related 7) deficiency did not suppress mitochondrial autophagy in E2-treated cells. Conversely, E2 increased the colocalization of Rab9 with LAMP2 (lysosomal-associated membrane protein 2) signals. The E2-mediated effects on mitochondrial autophagy were abolished by the knockdown of either Ulk1 or Rab9. These results suggest that E2-mediated mitochondrial autophagy is associated with Rab9-dependent alternative autophagy. E2 upregulated SIRT1 (sirtuin 1) and activated LKB1 (liver kinase B1), AMPK (adenosine monophosphate-activated protein kinase), and Ulk1, indicating that the effect of E2 on the induction of Rab9-dependent alternative autophagy is mediated by the SIRT1/LKB1/AMPK/Ulk1 pathway. Compared with the sham-operated mice, ovariectomized mice showed reduced mitochondrial autophagy and accelerated mitochondrial dysfunction and arterial senescence; these detrimental alterations were successfully rescued by the administration of E2.

CONCLUSIONS: We showed that E2-induced mitochondrial autophagy plays a crucial role in the delay of vascular senescence. The Rab9-dependent alternative autophagy is behind E2-induced mitochondrial autophagy.

Key Words: autophagy ■ estrogen ■ mitochondria ■ vascular senescence

Aging is a process involving physical, psychological, and social changes that ultimately affect life expectancy. For instance, it is associated with changes in multiple endocrine hormones such as androgens and estrogens. In particular, estrogen plays a crucial role in the maintenance of health and of the normal functioning of several organs such as muscles, bones, the brain, and the heart. Reduced endogenous estrogen levels are known to cause muscle loss,¹

osteoporosis,² Alzheimer's disease,³ and cardiovascular disease (CVD) in postmenopausal women. CVD is the leading cause of death among the older population in the world. Of note, premenopausal women have a lower mortality risk due to CVD than that of age-matched men in the United States, which is attributed to the vasculature protective effect of estrogen.^{4,5} The relationship between CVD and menopause was shown in the Framingham cohort; postmenopausal

Correspondence to: Yoshiyuki Ikeda, Department of Cardiovascular Medicine and Hypertension, Graduate School of Medical and Dental Sciences, 8-35-1 Sakuragaoka, Kagoshima 890-8520, Japan. E-mail: altezza@m2.kufm.kagoshima-u.ac.jp

Supplementary Material for this article is available at <https://www.ahajournals.org/doi/suppl/10.1161/JAHA.120.019310>

For Sources of Funding and Disclosures, see page 17.

© 2021 The Authors. Published on behalf of the American Heart Association, Inc., by Wiley. This is an open access article under the terms of the Creative Commons Attribution-NonCommercial-NoDerivs License, which permits use and distribution in any medium, provided the original work is properly cited, the use is non-commercial and no modifications or adaptations are made.

JAHA is available at: www.ahajournals.org/journal/jaha

CLINICAL PERSPECTIVE

What Is New?

- Estrogen regulates mitochondrial autophagy, which contributes to mitochondrial quality control and retards cellular senescence.
- Rab9-dependent alternative autophagy, but not Atg7/LC3 (autophagy related 7/light chain 3)-dependent conventional autophagy, is a predominant form of estrogen-induced mitochondrial autophagy.
- The effect of estrogen on inducing alternative autophagy is mediated by the SIRT1/LKB1/AMPK/ULK1 (sirtuin 1/liver kinase B1/adenosine monophosphate-activated protein kinase) pathway.

What Are the Clinical Implications?

- Our finding may contribute to develop new therapeutic approach, such as some techniques to induce Rab9 clinically, to inhibit atherosclerotic cardiovascular diseases in postmenopausal women.

Nonstandard Abbreviations and Acronyms

E2	17 β -estradiol
HUVECs	human umbilical vein endothelial cells
LAMP2	lysosome-associated membrane protein 2
OVX	ovariectomy
OXPPOS	oxidative phosphorylation
SMCs	smooth muscle cells
TOMM20	translocase of outer mitochondrial membrane 20

women had 2 to 6 times higher incidence of CVD than premenopausal women of the same age.⁶ Estrogens, particularly 17 β -estradiol (E2), have been used as the main constituents of hormone replacement therapy in postmenopausal women. A recent study showed that oral estradiol therapy initiated within 6 years of the menopause onset retarded subclinical atherosclerosis compared with that initiated after 10 or more years of menopause.⁷

Damaged organelles and abnormal proteins accumulate during the aging process; this disrupts cellular homeostasis.^{8–10} Recently, autophagy was proved as an important mechanism for maintaining cellular homeostasis via the elimination of damaged organelles, including mitochondria, proteins, and intracellular pathogens.^{11,12} Several studies have shown that

age-related deficit of autophagy was related to vascular senescence, potentially contributing to endothelial dysfunction, arterial stiffness, and vascular pathologies such as atherosclerosis and calcification.^{13,14} Therefore, interventions aiming to increase autophagy may reciprocally reduce age-related cardiovascular disease. Furthermore, although the relationship between estrogen and autophagy has been recently reported in tumor cells and neurons, few studies are available in the context of the vasculature.¹⁵

Mitochondria are essential organelles that supply ATP as energy in cells. Dysfunctional mitochondria accumulate with age, leading to reduced respiratory chain efficacy and ATP production and increased reactive oxygen species production, thereby facilitating cellular senescence.¹⁶ Aging may be affected by the increased reactive oxygen species levels in the vasculature.^{17,18} Because damaged mitochondria cause catastrophic consequences, mitochondrial quality control is important and modulated by various mechanisms. One of these mechanisms is organelle-specific autophagy; in particular, damaged mitochondria are degraded via autophagy.^{19,20} Estrogen-mediated mitophagy has been reported to be involved in various cell fates and human diseases.²¹ However, few studies have investigated the effects of estrogen on mitochondrial quality control via autophagy in the cardiovascular system.

Therefore, we hypothesized that the estrogen-mediated protection of the arteries from senescence and atherosclerosis is attributed to the induction of autophagy, especially mitochondrial autophagy. This study aimed to test this hypothesis.

METHODS

The authors declare that all supporting data are available within the article and its online supplementary files. An expanded Methods section is available in Data S1. Autophagy and mitochondrial autophagy were analyzed using electron microscopy, immunohistochemistry, and immunoblots with antibodies against LC3 (light chain 3) (MBL, M186-3), p62 (SQSTM1; MBL, PM045), Ulk1 (Abcam, ab128859), LAMP2 (lysosome-associated membrane protein 2; Sigma, L0668), TOMM20 (translocase of outer mitochondrial membrane 20; Abcam, ab186734), and Rab9 (Abcam, ab2810).

Cell Lines and Culture Methods

Human umbilical vein endothelial cells (HUVECs) and human aortic smooth muscle cells (SMCs) were purchased from Lonza Group Ltd. (Basel, Switzerland). When the cells reached 80% confluency, the culture medium was replaced with phenol red-free Dulbecco's modified Eagle's Medium (DMEM; GIBCO, Invitrogen) containing 10% charcoal-stripped fetal bovine serum

(Biowest) and maintained for 24 hours before E2 treatment. Because phenol red itself is known to possess estrogenic properties,^{22,23} incubation with phenol red-free medium represents the postmenopausal condition.

Cell Treatment

Cells were treated with 10 nmol/L E2 in phenol red-free DMEM supplemented with 2% charcoal-stripped fetal bovine serum. Control cells were exposed to the same volume of medium without E2. For the inhibition experiments performed using ICI 182780 (Sigma), sirtinol (Sigma), and Compound C (Sigma), new DMEM supplemented with 2% charcoal-stripped fetal bovine serum was added and maintained for 30 minutes, 1, 3, 6, and 24 hours before the addition of the inhibitors: ICI 182780 (1 μ mol/L), sirtinol (50 μ mol/L), Compound C (10 μ mol/L), or G15 (2 μ mol/L; Cayman).

Animal Models

All animal experiments were conducted in compliance with the protocol reviewed by the Institutional Animal Care and Use Committee and approved by the Faculty of Medicine, Kagoshima University, and followed the recommendations of the guidelines for animal experimentation at research institutes (Ministry of Education, Culture, Sports, Science and Technology, Japan and Ministry of Health, Labor and Welfare, Japan) and the guidelines for the proper conduct of animal experimentation (Science Council of Japan). Twelve-week-old female C57BL/6 mice were anesthetized with a combination of 0.3 mg/kg medetomidine, 4.0 mg/kg midazolam, and 5.0 mg/kg butorphanol by intraperitoneal injection (i.p.) and subjected in a random and allocation concealment fashion to bilateral ovariectomy (OVX) or sham surgery as described previously.²⁴ Body weight and food intake were measured every week after the surgery. The effects of E2 were determined via the subcutaneous implantation of E2 pellets or control pellets into OVX in mice (0.5 mg per pellet releasing 8.3 μ g/day; Innovative Research; OVX+E2), for 8 weeks, as previously described.²⁴

Statistical Analysis

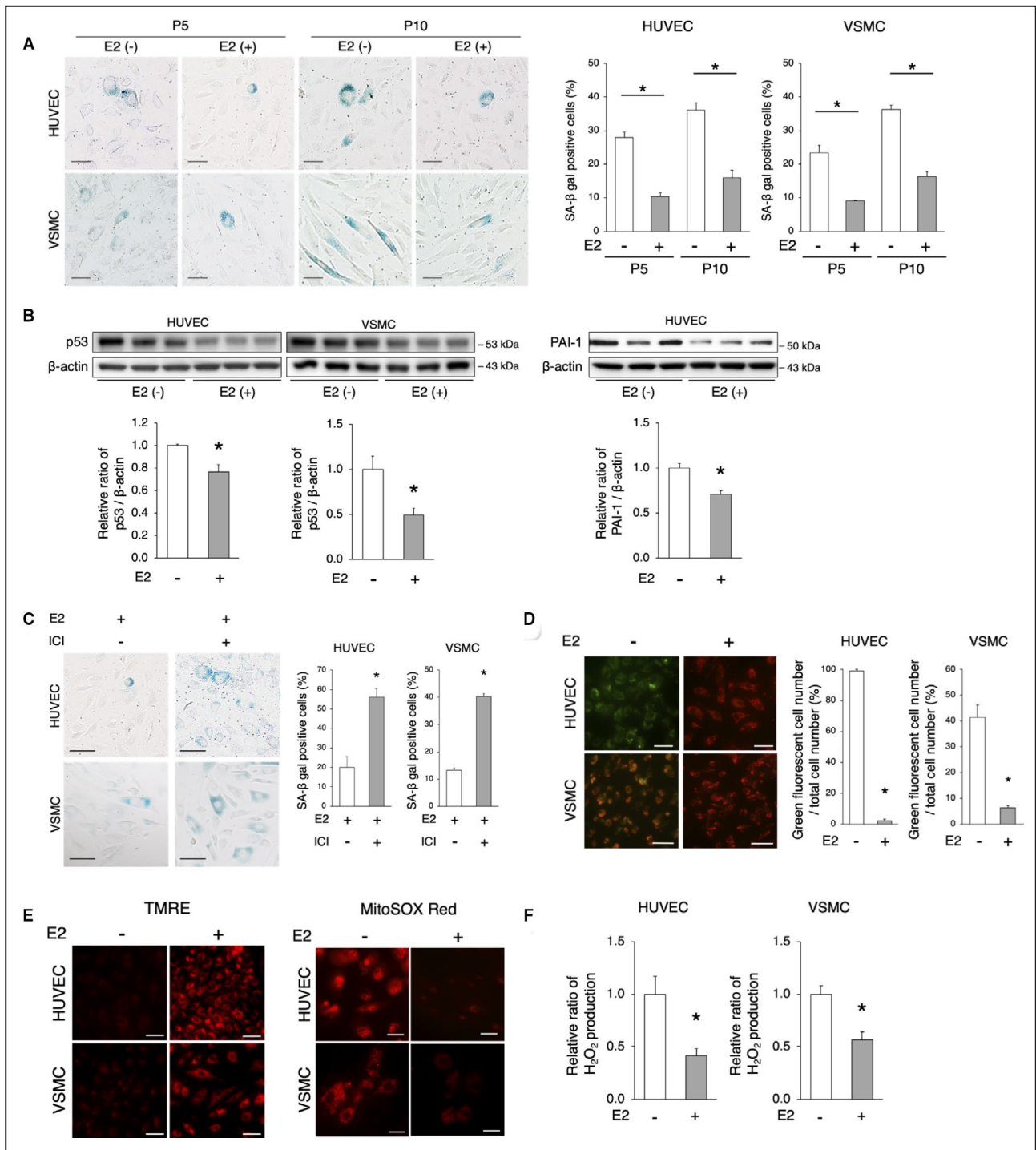
Data are expressed as the mean \pm SEM. The Student's *t* test was used to determine the statistical significance of differences between 2 groups. For data sets with a skewed distribution or smaller sample size ($n=3$ to 5 per group), the nonparametric statistical analysis was performed using the Wilcoxon rank sum test. Exceptions were the data in Figure 1A, 2E and 2F, and Figure S1B that were analyzed by 2-way analysis of variance. Analyses were performed by JMP Pro

15 (SAS Institute, Cary, NC, USA). *P* values < 0.05 were considered significant.

RESULTS

Estrogen-Protected HUVECs and Vascular SMCs from Senescence and Maintained Mitochondrial Function

We investigated the effects of estrogen on cellular senescence. Cellular senescence in HUVECs and vascular SMCs (VSMCs) was estimated using SA- β gal (senescence-associated β -galactosidase) staining. Premature senescence was induced under estrogen-free conditions and was accelerated in the context of increasing cell passages; importantly the administration of E2 delayed cell senescence (Figure 1A). There was no significant interaction between the cell passages and estrogen effects in HUVECs and VSMCs (HUVECs, *P* for interaction=0.48; VSMCs, *P* for interaction=0.06; Figure 1A). In addition, p53 expression was lower in both E2-treated HUVECs and VSMCs versus untreated control cells (Figure 1B). The expression of PAI-1 (plasminogen activator inhibitor-1) was also lower in E2-treated HUVECs than that in untreated control cells (Figure 1B). The effect of E2 on the delay of cellular senescence was abolished by the administration of the estrogen receptor inhibitor ICI 182780 (Figure 1C). Of note, the expression of p53 was increased according to the increase in cell passages in E2-treated VSMCs and HUVECs, and ICI 182780 treatment further promoted cellular senescence in E2-treated passage 10 VSMCs and HUVECs (Figure S1A). These results suggest that estrogen plays a crucial role in the regulation of cellular senescence. The mitochondrial membrane potential was evaluated via the staining of JC-1: polarized and depolarized mitochondria are marked by red and green fluorescence, respectively. E2-treated HUVECs and VSMCs showed a significantly lower number of cells with depolarized mitochondria than that in untreated cells (Figure 1D). Moreover, the number of cells with depolarized mitochondria was lower in E2-treated VSMCs and HUVECs treated with ICI 182780, and similar findings were observed in cells from advanced passages (Figure S1B). There was statistically 2-way interaction between the cell passages and ICI 182780 effects in E2 treated VSMCs and HUVECs (VSMCs, *P* for interaction=0.0004; HUVECs, *P* for interaction < 0.0001; Figure S1B). Tetramethylrhodamine ethyl ester staining also showed that E2 treatment in HUVECs and VSMCs maintained the mitochondrial membrane potential (Figure 1E). The intensity of MitoSox Red fluorescence was lower in both HUVECs and VSMCs treated with E2 (Figure 1E). H₂O₂ production assessed using Amplex Red was



also significantly lower in E2-treated versus untreated cells (Figure 1F). These data indicate that E2 maintains the mitochondrial function.

E2-Induced Mitochondrial Autophagy

A critical pathological feature of the aging process is the development of mitochondrial abnormalities; mitochondria are degraded by mitochondria-targeted

autophagy to maintain the overall mitochondrial health. Therefore, we investigated whether E2 regulates mitochondrial autophagy. Electron microscopic analysis showed that mitochondrial autophagy was higher in both HUVECs and VSMCs after E2 treatment than in those without E2 treatment (Figure 2A). Immunohistochemistry analysis showed that the colocalization of TOMM20 and LAMP2 signals was higher in both HUVECs and VSMCs treated with E2 than in

Figure 1. Estrogen treatment delays cellular senescence and maintains mitochondrial function in HUVECs and VSMCs.

A, Representative images of SA- β gal staining are shown. SA- β gal-positive cells increased with the increase in cell passages. The administration of E2 (10 nmol/L) decreased SA- β gal-positive cells. Scale bar=50 μ m. * P <0.01 vs E2(-) (n=5 per group). Statistical analysis was performed using 2-way analysis of variance. **B**, Immunoblots, and quantitative analysis results of p53, PAI-1, and β -actin are shown. The protein expression of p53 and PAI-1 were lower in E2-treated cells vs untreated cells. * P <0.05 vs E2(-) (n=3 per group). **C**, Representative images of SA- β gal staining of passage 5 cells treated with E2 (10 nmol/L)+ICI 182780 (1 μ mol/L) are shown. The administration of ICI attenuated the E2-mediated delay of cellular senescence. Scale bar, 50 μ m. * P <0.01 vs E2 (n=5 per group). **D**, Mitochondrial membrane potential was evaluated using JC-1. Red indicates mitochondria in which the membrane potential is maintained, whereas green indicates depolarized mitochondria. The quantification of HUVECs and VSMCs with depolarized mitochondria is shown. Scale bar, 50 μ m. * P <0.01 vs E2 (HUVECs, n=3 per group; VSMCs, n=5 per group). **E**, Left panel: TMRE staining for the assessment of mitochondrial membrane potential. Red indicates polarized mitochondria in which the membrane potential is maintained. Scale bar, 50 μ m. Right panel: Mitochondrial ROS was evaluated using MitoSox Red. The level of mitochondrial ROS, as red signals, was lower in E2-treated cells (n=4 per group). Scale bar, 25 μ m. **F**, H₂O₂ production in HUVECs and VSMCs treated with or without E2 was evaluated using the Amplex Red Assay. * P <0.01 (HUVECs, n=3 per group; VSMCs, n=4 per group). All data are shown as the mean \pm SEM. E2 indicates 17 β -estradiol; HUVECs, human umbilical vein endothelial cells; PAI-1, plasminogen activator inhibitor-1; ROS, reactive oxygen species; SA- β gal, senescence-associated β -galactosidase; TMRE, tetramethylrhodamine ethyl ester; and VSMCs, vascular smooth muscle cells.

those without E2 treatment (Figure 2B). Taken together, these results indicate that E2 promotes mitochondrial autophagy. Because the transition of LC3I to LC3II is crucial for the formation of autophagosomes, we determined the ratio of LC3II to LC3I in both HUVECs and VSMCs using western blot. E2 slightly, but not significantly, increased the ratio of LC3II to LC3I and decreased the expression of p62, which was degraded by autophagy (Figure 2C). Immunohistochemistry revealed that the number of LC3 signals that colocalized with LAMP2 signals was comparable between E2-treated and untreated VSMCs (Figure 2D). The number of LC3 signals that colocalized with TOMM20 signals was also comparable between E2-treated and untreated VSMCs (Figure 2D). Because ATG7 (autophagy related 7) plays a role in the regulation of LC3-dependent autophagy, we knocked down ATG7 in cultured VSMCs via transduction with an Atg7-targeting siRNA (Figure S2A) and investigated TOMM20 and LAMP2 via immunohistochemistry. The number of TOMM20 signals colocalizing with LAMP2 signals was comparable between siATG7- and siControl transduced VSMCs in the presence or absence of E2 (Figure 2E). There was no significant interaction between the siATG7 and estrogen effects (P for interaction=0.72; Figure 2E). Moreover, the mitochondrial autophagy number was not different between siATG7- and siControl-transduced VSMCs treated with or without E2 (Figure 2F). There was no significant interaction between the siATG7 and estrogen effects (P for interaction=0.83; Figure 2F). These results suggest that E2 induces mitochondrial autophagy, independently of ATG7.

E2-Induced Rab9-Dependent Alternative Autophagy in HUVECs and VSMCs

Recent studies have revealed a different form of autophagy in cardiomyocytes and mouse embryonic fibroblasts, called “alternative autophagy,” which is independent of ATG7 and LC3; it requires Ulk1,

followed by recruitment of the membrane trafficking protein Rab9.^{25,26} In contrast to alternative autophagy, ATG7- and LC3-dependent autophagy is called “conventional autophagy.” Immunohistochemistry of Rab9 and LAMP2 in HUVECs and VSMCs showed that E2 increased the number of LAMP2 signals colocalized with Rab9 signals in both cell types (Figure 3A). Next, we knocked down Rab9 in cultured VSMCs and performed electron microscopy and immunohistochemistry analyses (Figure S2B). Electron microscopy showed that mitochondrial autophagy in E2-treated VSMCs was decreased in the context of Rab9 knockdown (Figure 3B). Immunohistochemistry further revealed that the number of Rab9 – LAMP2 colocalized signals was lower in E2-treated VSMCs transduced with siRab9 versus those transduced with siControl (Figure 3C). The number of TOMM20 signals colocalized with LAMP2 signals was also lower in E2-treated VSMCs transduced with siRab9 than in those transduced with siControl (Figure 3D). To determine whether mitochondrial dysfunction was because of decreased levels of OXPHOS (oxidative phosphorylation) protein, we measured them. There were no significant changes in the expression of OXPHOS protein levels between E2-treated and untreated VSMCs (Figure S3A). E2-treated VSMCs transduced with siControl showed a significantly lower number of cells with depolarized mitochondria than in those transduced with siRab9, as per the staining of JC-1 (Figure S3B). Tetramethylrhodamine ethyl ester staining also showed that E2-treated VSMCs transduced with siControl maintained mitochondrial membrane potential, contrarily to VSMCs transduced with siRab9 (Figure S3C). Taken together, these results suggest that estrogen induces Rab9-dependent alternative autophagy, which may contribute to mitochondrial autophagy. Next, we knocked down Ulk1 in cultured VSMCs to determine whether Ulk1 mediates Rab9-dependent autophagy (Figure S2C). Immunohistochemistry revealed that

the number of Rab9 – LAMP2 colocalizing signals was lower in E2-treated VSMCs transduced with siUlk1 than in those transduced with siControl, suggesting that Rab9-dependent autophagy in VSMCs requires Ulk1 (Figure 3E). In myocardial ischemia, it has been reported that mitophagy is induced via the Ulk1-Rab9-Rip1-Drp1 pathway; of note, mitochondria dynamics is associated with mitophagy in various cardiovascular diseases.^{25,27} Therefore, we investigated the expression of phosphorylated Rip1 and Drp1, as well as of several factors involved mitochondrial dynamics. The expression of p-Drp1 (Ser616), p-Drp1 (Ser637), Drp1, Mfn1, Mfn2, Opa1, Rip1, and PGC1- α were not different in E2-treated versus untreated VSMCs (Figure S3D). Mitotracker also showed that the ratio of cells with fragmented mitochondria were not significantly different, comparing E2-treated and untreated VSMCs (Figure S3E). These results suggest that neither the Rab9-Rip1-Drp1 pathway nor mitochondria dynamics are involved in E2-induced mitochondrial autophagy.

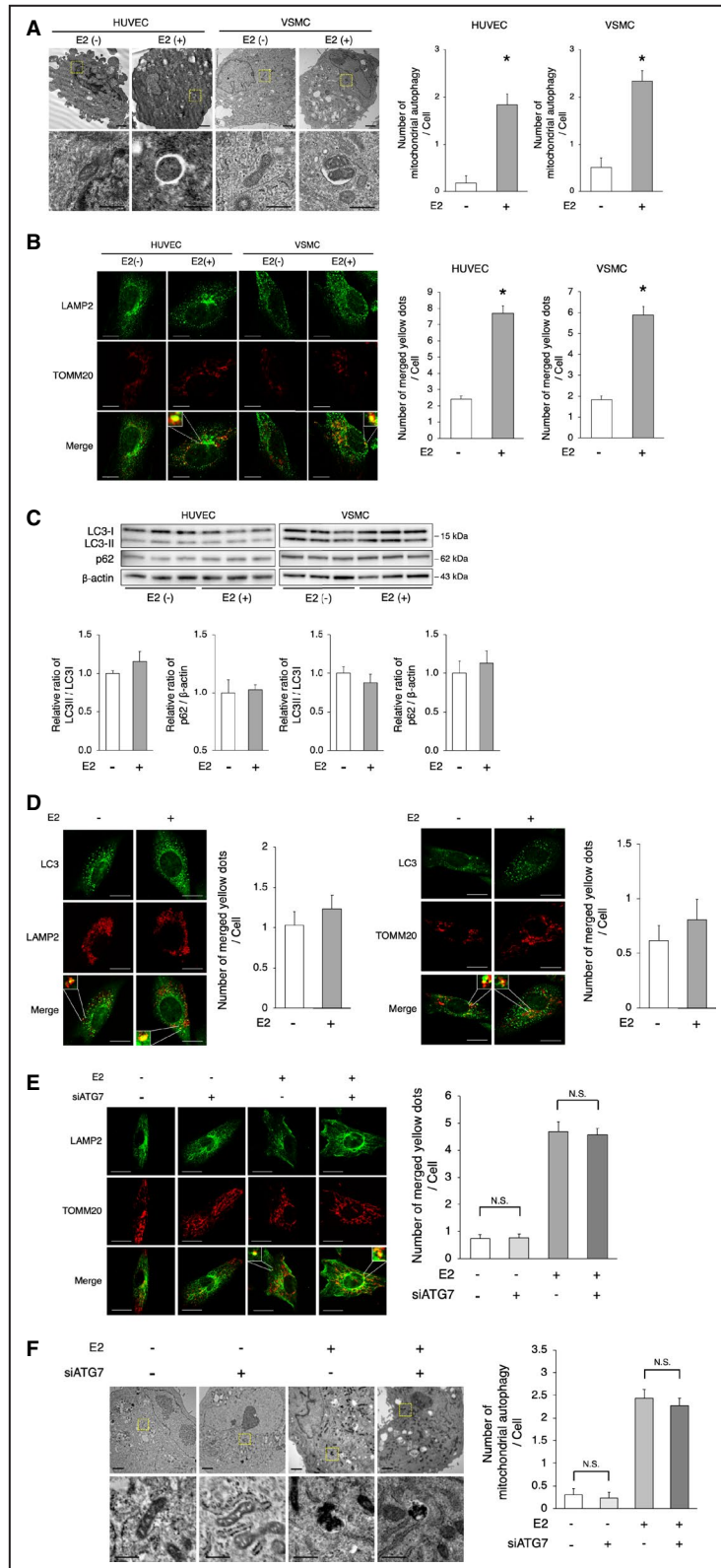
SIRT1-Regulated E2-Mediated Rab9-Dependent Alternative Autophagy

We investigated the potential mechanism behind E2-mediated alternative autophagy. The Sir2 (silent information regulator 2) protein (one of the sirtuins) has been shown to prolong the life span of yeast, whereas its deficiency induced the opposite results.²⁸ Increasing evidence suggests that SIRT1 (sirtuin1), a mammalian Sir2 homolog, has a close relationship with longevity. Furthermore, the activation

of SIRT1 leads to antiaging effects in the vasculature, reducing inflammation, oxidative stress, and DNA damage.²⁹ We previously showed that SIRT1 is regulated by estrogen and is involved in the etiology of menopause-induced arterial senescence and atherosclerosis in apolipoprotein E-knockout (ApoE KO) mice.²⁴ Therefore, we hypothesized that estrogen might induce autophagy via the activation of SIRT1. The expression of SIRT1 was higher in both HUVECs and VSMCs, whereas the administration of ICI 182780 abolished SIRT1 induction by E2 (Figure 4A and 4B, Figure S4A and S4B). Estrogen binds to 3 known estrogen receptors, ER α , ER β , and G protein-coupled estrogen receptor. We previously reported that estrogen upregulates the protein expression of SIRT1 via ER α ; therefore, we checked the involvement of G protein-coupled ER in this experiment. The administration of G15, which is a G protein-coupled ER antagonist, did not significantly change the expression of SIRT1 (Figure 4C). On the other hand, SIRT1 signaling inhibition using a SIRT1 inhibitor, sirtinol, deteriorated the effect of E2 on the delay of cellular senescence in VSMCs (Figure 4D). Taken together, these results suggest that estrogen prevents cellular senescence through the induction of SIRT1. Next, we investigated the relationship between alternative autophagy and SIRT1. Electron microscopy analysis showed that the number of mitochondria undergoing autophagy in the context of E2 stimulation was lower in sirtinol-treated versus control VSMCs (Figure 4E). Immunohistochemistry of Rab9 and LAMP2 in E2-treated VSMCs revealed that the number of LAMP2 – Rab9 colocalizing signals

Figure 2. E2-induced mitochondrial autophagy.

A, Electron microscopy analyses of mitochondrial autophagy in HUVECs and VSMCs with or without E2 (upper panel, scale bar=1 μ m). Enlarged images of the areas delineated by the dashed rectangles are shown below (scale bar=500 nm). The cells of each group were randomly selected from 3 independent experiments, and the number of mitochondria engulfed by autophagosomes was counted. The number of autophagosomes/autolysosomes engulfing mitochondria per cell was higher in E2-treated cells. * P <0.01 vs E2(-). **B**, Representative images of LAMP2 (green) and TOMM20 (red) immunohistochemistry in HUVECs and VSMCs with or without E2. Thirty cells were evaluated per group, in the context of 3 independent experiments. The number of merged yellow signals was higher in E2-treated cells. Scale bar=10 μ m. * P <0.01 vs E2(-). **C**, Immunoblots and quantitative analysis results of LC3 and p62 are shown. No difference in LC3 and p62 was noted between the 2 groups (n =3 per group). **D**, Left panel: Representative images of LC3 (green) and LAMP2 (red) immunohistochemistry in VSMCs with or without E2. Thirty cells were evaluated per group, in the context of 3 independent experiments. The number of merged yellow signals was not different between the 2 groups. Scale bar=10 μ m. Right panel: Representative images of LC3 (green) and TOMM20 (red) immunohistochemistry in VSMCs with or without E2. Thirty cells were evaluated per group, in the context of 3 independent experiments. The number of merged yellow signals was not different between the 2 groups. Scale bar=10 μ m. **E**, Representative images of LAMP2 (green) and TOMM20 (red) immunohistochemistry in E2 or vehicle-treated VSMCs transfected with siATG7 or siControl. Thirty cells were evaluated per group, in the context of 3 independent experiments. The number of merged yellow signals was not different in VSMCs transfected with siATG7 and siControl, either treated with vehicle or E2, respectively. N. S.; not significant. Statistical analysis was performed using 2-way analysis of variance. Scale bar=10 μ m. **F**, Electron microscopy analyses of mitochondrial autophagy in E2 or vehicle-treated VSMCs transfected with siATG7 or siControl (upper panel, scale bar, 1 μ m). Enlarged images of the areas delineated by the dashed rectangles are shown below (scale bar=500 nm). The cells of each group were randomly selected from 3 independent experiments, and the number of mitochondria engulfed by autophagosomes was counted. The number of autophagosomes/autolysosomes engulfing mitochondria per cell was not different in VSMCs transfected with siATG7 and siControl, either treated with vehicle or E2, respectively. N. S.; not significant. Statistical analysis was performed using 2-way analysis of variance. All data are shown as the mean \pm SEM. E2 indicates 17 β -estradiol; HUVECs, human umbilical vein endothelial cells; LAMP2, lysosome-associated membrane protein 2; LC3, light chain 3; TOMM20, translocase of outer mitochondrial membrane 20; and VSMCs, vascular smooth muscle cells.



was lower in VSMCs treated with sirtinol (versus control VSMCs; Figure 4F). In addition, immunohistochemistry showed that the number of LAMP2 and TOMM20 colocalizing signals was lower in VSMCs

treated with E2+sirtinol than in those treated with E2 alone (Figure 4G). Taken together, these results suggest that E2 upregulates SIRT1, which in turn regulates Rab9-dependent alternative autophagy.

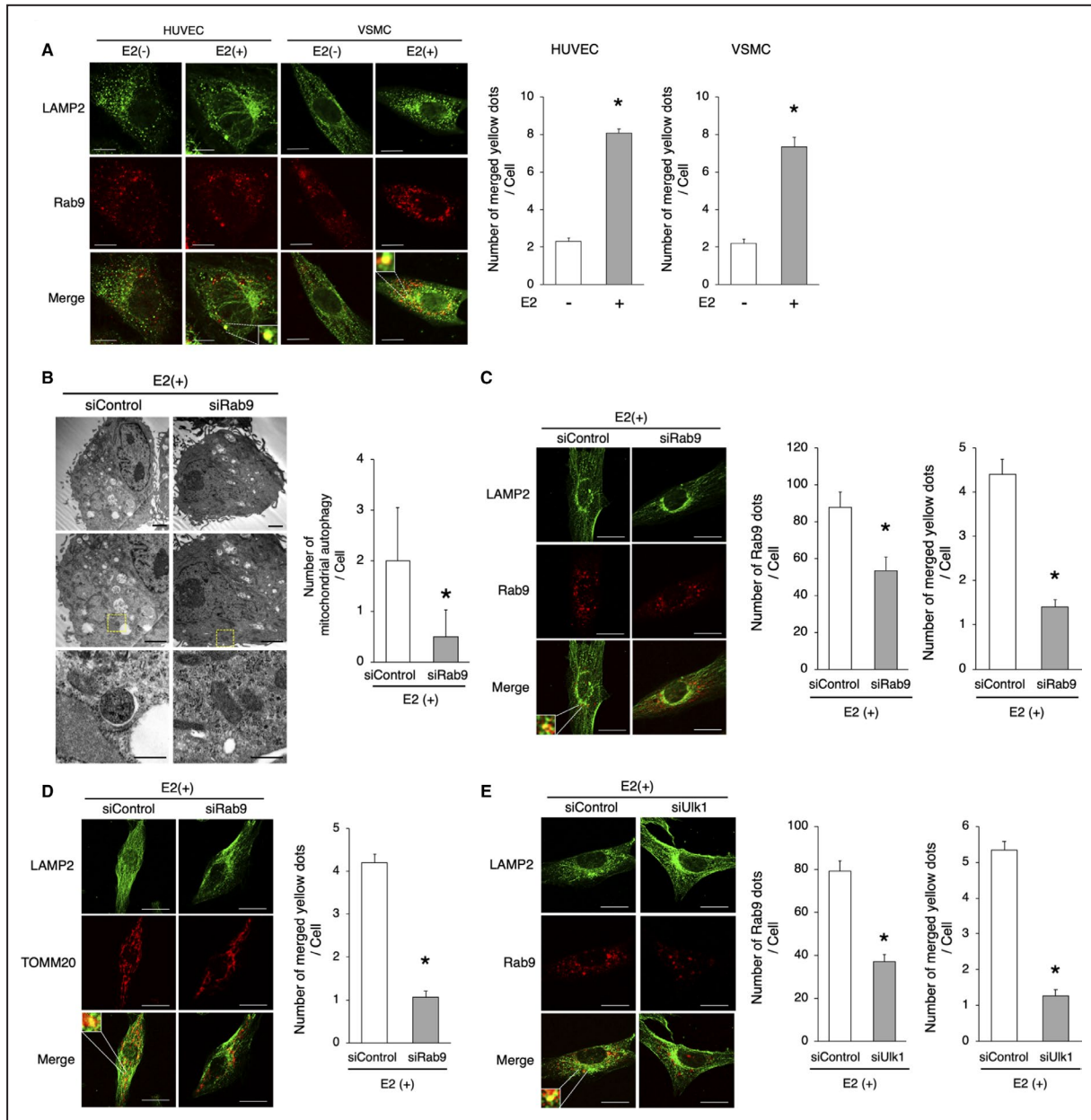


Figure 3. E2-induced Rab9-dependent alternative autophagy.

A, Representative images of LAMP2 (green) and Rab9 (red) immunohistochemistry in HUVECs and VSMCs with or without E2. Thirty cells were evaluated per group, in the context of 3 independent experiments. The number of merged yellow signals was higher in E2-treated cells. $*P < 0.01$ vs E2(-). Scale bar=10 μ m. **B**, Electron microscopy analyses of mitochondrial autophagy in E2-treated VSMCs transfected with siRab9 or siControl (upper and middle panel, respectively, scale bar, 1 μ m). Enlarged images of the areas delineated by the dashed rectangles are shown below (scale bar, 500 nm). The cells of each group were randomly selected from 3 independent experiments, and the number of mitochondria engulfed by autophagosomes was counted. The number of autophagosomes/autolysosomes engulfing mitochondria per cell was lower in E2-treated cells transfected with siRab9. $*P < 0.01$ vs siControl. **C**, Representative images of LAMP2 (green) and Rab9 (red) immunohistochemistry in E2-treated VSMCs transfected with siRab9. Thirty cells were evaluated per group, in the context of 3 independent experiments. The number of Rab9 signals and merged yellow signals was lower in E2-treated cells transfected siRab9. Scale bar, 10 μ m. $*P < 0.01$ vs siControl. **D**, Representative images of LAMP2 (green) and TOMM20 (red) immunohistochemistry in E2-treated VSMCs transfected with siRab9. Thirty cells were evaluated per group, in the context of 3 independent experiments. The number of merged yellow signals was lower in E2-treated cells transfected with siRab9. Scale bar, 10 μ m. $*P < 0.01$ vs siControl. **E**, Representative images of LAMP2 (green) and Rab9 (red) immunohistochemistry in E2-treated VSMCs transfected with siUlk1. Thirty cells were evaluated per group, in the context of 3 independent experiments. The number of Rab9 signals and merged yellow signals was lower in E2-treated cells transfected with siUlk1. Scale bar, 10 μ m. $*P < 0.01$ vs siControl. All data are shown as the mean \pm SEM. E2 indicates 17 β -estradiol; HUVECs, human umbilical vein endothelial cells; LAMP2, lysosome-associated membrane protein 2; TOMM20, translocase of outer mitochondrial membrane 20; and VSMCs, vascular smooth muscle cells.

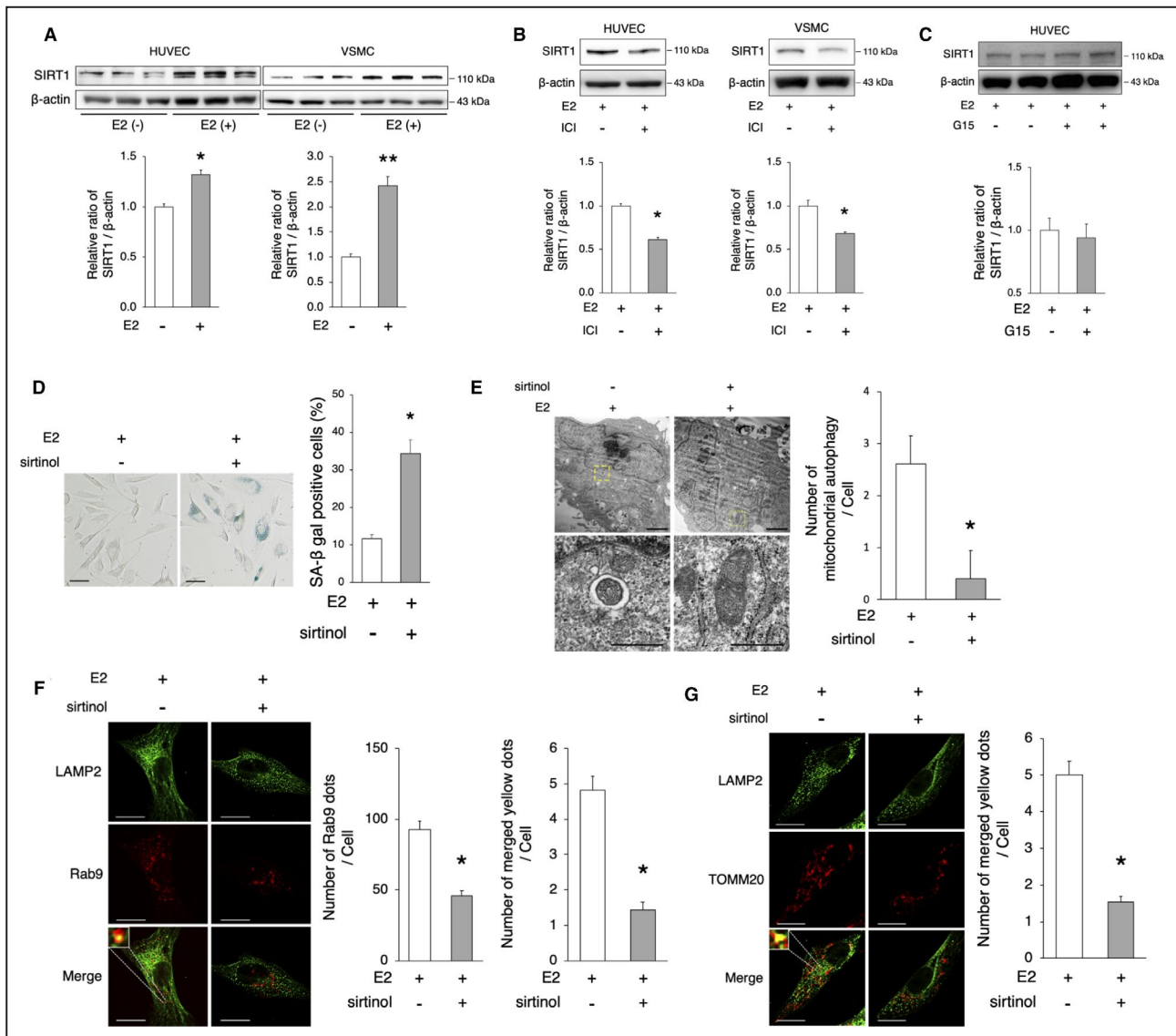


Figure 4. SIRT1 regulates E2-mediated Rab9-dependent alternative autophagy.

A, Immunoblots and quantitative analysis results of SIRT1 are shown. SIRT1 protein expression was higher in E2-treated cells vs untreated cells. * $P < 0.05$ vs E2(-); ** $P < 0.01$ vs E2(-) ($n = 3$ per group). **B**, Representative immunoblots and quantitative analysis results of E2-treated HUVECs and VSMCs with or without ICI 182780 (1 $\mu\text{mol/L}$) are shown. ICI 182780 decreased the protein expression of SIRT1. * $P < 0.05$ vs E2(+) (HUVECs, $n = 3$ per group; VSMCs, $n = 4$ per group). **C**, Representative immunoblots and quantitative analysis results of E2-treated HUVECs with or without G15 (20 $\mu\text{mol/L}$) are shown. G15 did not change the protein expression of SIRT1 ($n = 4$ per group). **D**, Representative images of SA- β gal staining of cells treated with E2 (10 nmol/L)+sirtinol (50 $\mu\text{mol/L}$) are shown. The number of SA- β gal-positive cells was increased after the administration of sirtinol. Scale bar, 50 μm . * $P < 0.05$ vs E2(+) ($n = 5$ per group). **E**, Electron microscopy analyses of mitochondrial autophagy in E2-treated VSMCs with or without sirtinol (upper panel, scale bar, 1 μm). Enlarged images of the areas delineated by the dashed rectangles are shown below (scale bar, 500 nm). The cells of each group were randomly selected from 3 independent experiments, and the number of mitochondria engulfed by autophagosomes was counted. The number of autophagosomes/autolysosomes engulfing mitochondria per cell was lower in E2-treated cells with sirtinol. * $P < 0.01$ vs E2(+). **F**, Representative images of LAMP2 (green) and Rab9 (red) immunohistochemistry in E2-treated VSMCs with sirtinol. Thirty cells were evaluated per group, in the context of 3 independent experiments. The number of Rab9 signals and merged yellow signals was lower in E2-treated cells with sirtinol. Scale bar, 10 μm . * $P < 0.01$ vs E2(+). **G**, Representative images of LAMP2 (green) and TOMM20 (red) immunohistochemistry in E2-treated VSMCs with sirtinol. Thirty cells were evaluated per group, in the context of 3 independent experiments. The number of merged yellow signals was lower in E2-treated cells with sirtinol. Scale bar, 10 μm . * $P < 0.01$ vs E2(+). All data are shown as the mean \pm SEM. E2 indicates 17 β -estradiol; HUVECs, human umbilical vein endothelial cells; LAMP2, lysosome-associated membrane protein 2; SA- β gal, senescence-associated β -galactosidase; SIRT1, sirtuin 1; TOMM20, translocase of outer mitochondrial membrane 20; and VSMCs, vascular smooth muscle cells.

The SIRT1/LKB1/AMPK/ULK1 Axis Induced Alternative Autophagy

We also determined the precise mechanisms by which SIRT1 upregulates the Rab9-dependent alternative autophagy pathway. Several recent studies revealed that SIRT1 activates AMPK (adenosine monophosphate-activated protein kinase) through LKB1 (liver kinase B1).³⁰ In addition, AMPK activation through the phosphorylation of Thr172 was reported to play a crucial role in the induction of Rab9-dependent alternative autophagy via the activation of Ulk1 (phosphorylation of ser555).²⁵ Here, E2 increased the expression of LKB1, p-LKB1 (Ser428), p-AMPK (Thr172), p-Ulk1 (Ser555), and Rab9 in VSMCs (Figure 5A). Moreover, the E2-mediated increase of LKB1, p-LKB1, p-AMPK, p-Ulk1, and Rab9 was abrogated by SIRT1 inhibition (Figure 5B). Furthermore, the same was true in the context of AMPK inhibition, using Compound C (Figure 5C). Of note, the number of Rab9 signals was lower in E2-treated VSMCs treated with Compound C versus control cells (Figure 5D). We also confirmed that SIRT1, LKB1, AMPK, Ulk1, and Rab9 were upregulated by E2 in HUVECs (Figure S5A–S5C). Taken together, these results suggest that E2 activates the SIRT1-LKB1-AMPK pathway accompanied by the activation of Ulk1, resulting in the induction of Rab9-dependent alternative autophagy.

Estrogen-Regulated Mitochondrial Autophagy and Arterial Senescence in Mice

We investigated whether OVX would promote arterial senescence in C57BL/6 female mice. Food intake during the experiment, body weight, and serum estradiol concentrations 8 weeks after surgery were not different between sham-operated and OVX mice (Table). These parameters were also not different between OVX mice administered E2 and those provided control pellets (Table). Arterial fibrosis, assessed using the Masson's trichrome staining was increased in OVX mice compared with that in sham-operated mice (Figure 6A). Arterial 4-hydroxynonenal immunoreactivity and the H₂O₂ production in the context of isolated mitochondria from the aorta were higher in OVX mice than in sham-operated mice, suggesting that OVX increased oxidative stress in the arteries (Figure 6B and 6C). Immunoblot analysis revealed that the arterial expression of Ac-p53 was also higher in OVX versus sham-operated mice (Figure 6D). Electron microscopy analysis showed that mitochondrial autophagy was significantly lower in OVX mice than that in sham-operated mice (Figure 6E). Immunohistochemistry revealed that the number of TOMM20 - LAMP2 colocalizing signals was significantly lower in OVX versus sham-operated

mice (Figure 6F). The expression of p-Ulk1 (Ser555) and Rab9 was also lower in OVX mice than that in sham-operated mice (Figure 6G). In addition, the number of Rab9 - LAMP2 colocalizing signals was significantly lower in OVX versus sham-operated mice (Figure 6H). On the other hand, the ratio of LC3II to LC3I and the expression of p62 were not different between sham-operated and OVX mice (Figure 6I). Taken together, these results suggest that the OVX-induced decrease of estrogen diminishes mitochondrial autophagy, leading to the decrease of mitochondrial function and the consequent acceleration of arterial senescence. Next, we conducted experiments using female Young mice and Old mice to investigate whether similar results would be observed in function of age. Arterial fibrosis, assessed using the Masson's trichrome staining, was increased in Old mice compared with that in Young mice (Figure S6A). Electron microscopy analysis showed that mitochondrial autophagy was significantly lower in Old versus Young mice (Figure S6B). The expression of p-Ulk1 (Ser555) and Rab9 was also lower in Old versus Young mice (Figure S6C). Moreover, immunohistochemistry revealed that the number of Rab9 - LAMP2 colocalizing signals was lower in Old mice (Figure S6D). Conversely, ATP production was lower in Young versus Old mice (Figure S6E). Of note, the ratio of LC3II to LC3I and the expression of p62 were not different between Young and Old mice (Figure S6F). These results suggest that in Old mice, as in OVX mice, the reduction of Rab9-dependent mitochondrial autophagy induces arterial senescence. We performed rescue experiments using OVX mice implanted with either E2 pellets or control pellets for 8 weeks. Compared with OVX mice implanted with control pellets (OVX+Ctr), OVX mice implanted with E2 pellets (OVX+E2) showed retarded arterial fibrosis, as per the Masson's trichrome staining (Figure 7A). Arterial 4-hydroxynonenal immunoreactivity and the production of H₂O₂ by mitochondria isolated from the aorta were lower in OVX+E2 mice than in OVX+Ctr mice, suggesting that OVX+E2 decreased oxidative stress in the arteries (Figure 7B and 7C). Immunoblot analysis revealed that the expression of Ac-p53 was lower in OVX+E2 mice than that in OVX+Ctr mice (Figure 7D). Electron microscopy analysis revealed that mitochondrial autophagy was higher in OVX+E2 mice than that in OVX+Ctr mice (Figure 7E). The number of TOMM20 - LAMP2 and Rab9 - LAMP2 colocalizing signals was significantly higher in OVX+E2 versus OVX+Ctr mice (Figure 7F and 7G). The expression of p-Ulk1 (Ser555) and Rab9 was also higher in OVX+E2 versus OVX+Ctr mice (Figure 7H). The expression of OXPHOS was slightly lower in OVX+E2 mice than that in OVX+Ctr mice; however, the difference in the protein levels was not significant (Figure 7I). On the other hand, ATP production was higher in OVX+E2 versus

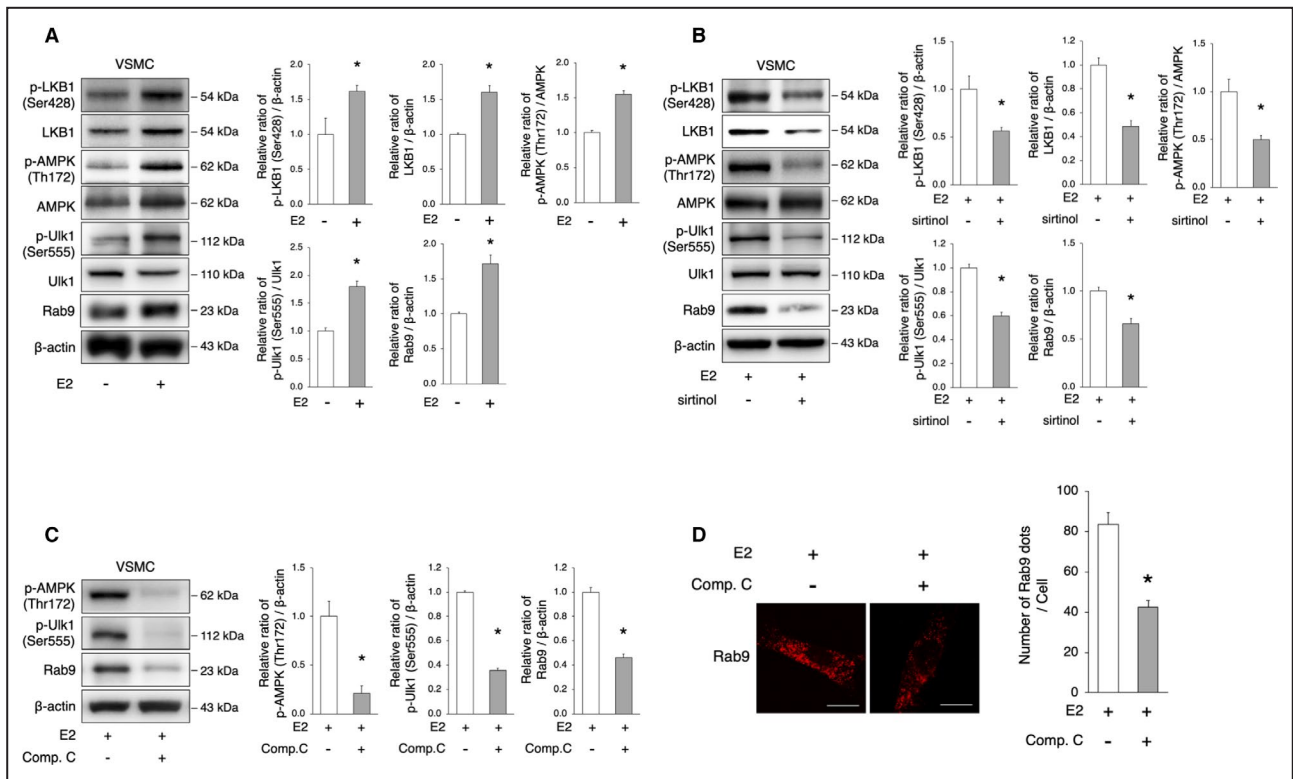


Figure 5. The SIRT1/LKB1/AMPK/UIk1 axis is involved in the induction of alternative autophagy.

A, Representative immunoblots and quantitative analysis of LKB1, AMPK, UIk1, and Rab9 in VSMCs with or without E2 treatment. E2 treatment activated LKB1, AMPK, UIk1, and Rab9. * $P < 0.05$ vs E2(-) (n=3 per group). **B**, Representative immunoblots and quantitative analysis of LKB1, AMPK, UIk1, and Rab9 in E2-treated VSMCs with or without sirtinol. The administration of sirtinol attenuated the activation of LKB1, AMPK, UIk1, and Rab9 by E2. * $P < 0.05$ vs E2(+) (n=3 per group). **C**, Representative immunoblots and quantitative analysis of AMPK, UIk1, and Rab9 in E2-treated VSMC with or without Compound C (10 μ mol/L). The administration of Compound C attenuated the activation of AMPK, UIk1, and Rab9 by E2. * $P < 0.05$ vs E2(+) (n=3 per group). **D**, Representative images of Rab9 (red) immunohistochemistry in E2-treated VSMCs with Compound C (10 μ mol/L). Thirty cells were evaluated per group, in the context of 3 independent experiments. The number of Rab9 signals was lower in E2-treated cells with Compound C. Scale bar, 10 μ m. * $P < 0.01$ vs E2(+). All data are shown as the mean \pm SEM. AMPK indicates adenosine monophosphate-activated protein kinase; E2, 17 β -estradiol; LAMP2, lysosome-associated membrane protein 2; LKB1, liver kinase B1; SIRT1, sirtuin 1; and VSMCs, vascular smooth muscle cells.

OVX+Ctr mice (Figure 7J). These results suggest that E2-induced mitochondrial autophagy contributes to the maintenance of mitochondrial function. Of note, the ratio of LC3II to LC3I and the expression of p62 was not different between OVX+E2 mice and OVX+Ctr mice (Figure S7A). On the other hand, the administration of 3-Methyladenine, a PI3K (phosphoinositide 3-kinase) inhibitor commonly used as an autophagy inhibitor, decreased LC3II levels in OVX+E2 mice (Figure S7B). However, electron microscopy analysis showed that the administration of 3-Methyladenine did not affect mitochondrial autophagy in OVX+E2

mice (Figure S7C). Additionally, the administration of 3-Methyladenine did not significantly change the expression of senescence markers in OVX+E2 mice (Figure S7D). These results indicate that E2-induced mitochondrial autophagy is not derived from conventional autophagy. We further performed experiments using female ApoE KO mice, a model of atherosclerosis, to investigate whether Rab9-dependent mitochondrial autophagy is involved in the exacerbation of vascular pathology. Of note, we previously reported that in ApoE KO mice, OVX promotes arterial senescence and atherosclerosis, whereas estradiol

Table. Body Weight, Food Intake, and Serum Estradiol Levels

	Sham (n=7)	OVX (n=7)	P Value	OVX (n=6)	OVX+E2 (n=6)	P Value
Body weight, g	29.1 \pm 1.8	31.2 \pm 1.1	0.08	31.1 \pm 0.9	30.2 \pm 1.4	0.22
Food intake, g/day	4.6 \pm 0.2	4.5 \pm 0.1	0.29	4.4 \pm 0.2	4.7 \pm 0.1	0.10
Estradiol, pg/mL	23.4 \pm 9.9	5.8 \pm 2.2	0.05	7.3 \pm 2.4	22.2 \pm 6.2	0.05

All values are mean and SD. No animals died in the experiments. OVX indicates ovariectomy.

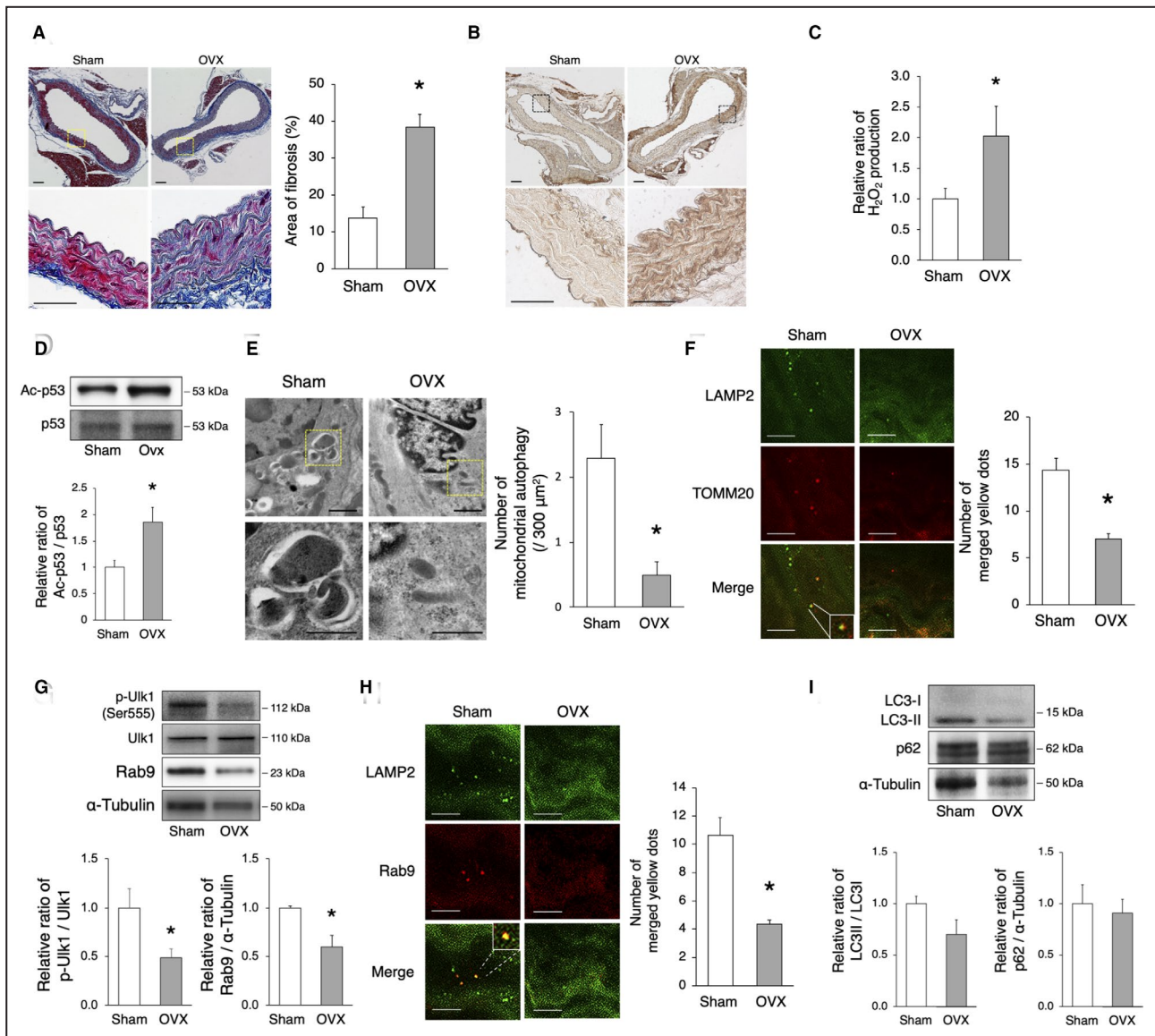


Figure 6. OVX promotes arterial senescence via the decrease of mitochondrial autophagy.

C57BL/6 mice were subjected to OVX or sham surgery. **A**, Assessment of aortic fibrosis in sham-operated and OVX mice using the Masson's trichrome staining 8 weeks after surgery. Enlarged images of the areas delineated by the dashed rectangles are shown below. The area of fibrosis was greater in OVX mice. Scale bar, 25 μm . $*P < 0.05$ vs sham ($n = 3$ per group). **B**, Representative images of 4-HNE in sham-operated and OVX mice. Immunoreactivity of 4-HNE increased in the aorta of OVX mice compared with that of sham-operated mice. **C**, The relative H_2O_2 production by isolated mitochondria from the aorta of sham-operated and OVX mice 8 weeks after surgery was evaluated using the Amplex Red Assay. H_2O_2 production was higher in OVX mice. $*P < 0.05$ vs sham ($n = 3$ per group). **D**, Representative immunoblots and quantitative analysis of Ac-p53 and p53 in sham-operated and OVX mice. The expression of Ac-p53 was higher in OVX mice than that in sham-operated mice. $*P < 0.05$ vs sham ($n = 4$ per group). **E**, Electron microscopy images of the aorta from sham-operated and OVX mice (upper panel, scale bar, 1 μm). Enlarged images of the areas delineated by the dashed rectangles are shown below (scale bar, 500 nm). More than 900 μm^2 of the aorta of each mouse were screened in a random fashion; 3 samples per group were evaluated and the number of mitochondria engulfed by autophagosomes was counted. The number of mitochondrial autophagy was lower in OVX mice. $*P < 0.05$ vs sham. **F**, Representative images of LAMP2 (green) and TOMM20 (red) immunohistochemistry of the aorta in sham-operated and OVX mice. The merged yellow signals were lower in OVX mice. Scale bar, 5 μm . $*P < 0.05$ vs sham ($n = 3$ per group). **G**, Representative immunoblots and quantitative analysis of Ulk1 and Rab9 in sham-operated and OVX mice. The expression of activated Ulk1 and Rab9 was higher in sham-operated vs OVX mice. $*P < 0.05$ vs sham ($n = 4$ per group). **H**, Representative images of LAMP2 (green) and Rab9 (red) immunohistochemistry of the aorta in sham-operated and OVX mice. The number of yellow signals was lower in OVX mice. Scale bar, 5 μm . $*P < 0.05$ vs sham ($n = 3$ per group). **I**, Representative immunoblots and quantitative analysis of LC3 and p62 in sham and OVX mice. The expression of both LC3 and p62 was not different between the 2 groups ($n = 4$ per group). All data are shown as the mean \pm SEM. 4-HNE indicates 4-hydroxynonenal; LAMP2, lysosome-associated membrane protein 2; LC3, light chain 3; OVX, ovariectomy; and TOMM20, translocase of outer mitochondrial membrane 20.

administration suppresses arterial senescence and atherosclerosis.²⁴ Here, immunoblot analysis showed that the expression of p-Ulk1 (Ser555) and Rab9 was lower in ApoE KO OVX versus sham-operated mice (Figure S8A). Immunohistochemistry further revealed that the number of Rab9 – LAMP2 colocalizing signals was significantly lower in ApoE KO OVX mice than that in sham-operated KO mice (Figure S8B). Again, the ratio of LC3II to LC3I and the expression of p62 were not different between sham and OVX ApoE KO mice (Figure S8C). Furthermore, the administration of E2 rescued p-Ulk1 (Ser555) and Rab9 expression and mitochondrial autophagy (Figure S8D and S8E); again, the administration of E2 did not change the LC3II levels (Figure S8F). Taken together, these results suggest that E2 regulates mitochondrial autophagy derived from Rab9-dependent alternative autophagy and maintains mitochondrial function, preventing arterial senescence and atherosclerosis.

DISCUSSION

Our findings suggest that estrogen regulates mitochondrial autophagy, which contributes to mitochondrial quality control and delays cellular senescence. Rab9-dependent alternative autophagy, but not Atg7/LC3-dependent conventional autophagy, is the predominant form of E2-induced mitochondrial autophagy. The effect of E2 on the induction of alternative autophagy is mediated by the SIRT1/LKB1/AMPK/Ulk1 pathway. The administration of E2 to C57BL/6 OVX mice restored mitochondrial autophagy through the Rab9-dependent alternative autophagy and delayed OVX-induced arterial senescence.

Estrogen-mediated autophagy and mitochondrial autophagy are involved in various cell fates and human diseases, such as osteoporosis, Hodgkin lymphoma, Parkinson's disease, osteoarthritis, and ischemic heart; of note, they play a protective role, maintaining cell homeostasis. However, few studies have investigated the relationship between estrogen-induced autophagy and the vasculature. In addition, which form of autophagy, conventional or alternative, contributes to mitochondrial quality control in the vasculature is not yet known. ATG5 and ATG7 are key molecules, and the conversion of LC3I to LC3II is vital to induce autophagy.^{31,32} However, recently, several studies showed the existence of alternative forms of autophagy, independent of ATG5, ATG7, and LC3. Nishida et al described that ATG5/ATG7-independent autophagosome formation in mouse embryonic fibroblasts appeared to be regulated by the small GTPase Rab9 and required Ulk1 in the initial step of autophagy induction.²⁶ ATG5/ATG7-dependent conventional autophagy that requires LC3

plays a crucial role in the degradation of unfolded and aged proteins and organelles, which contributes to the maintenance of tissue homeostasis. Conversely, alternative autophagy is remarkably involved in the prevention of cellular damage caused by various stressors.³³ In our study, the number of LAMP2 – Rab9 colocalizing signals and the number of autophagosome-engulfed mitochondria in both HUVECs and VSMCs were increased by E2. Of note, this phenotype was lost after the knockdown of either Rab9 or Ulk1 and was not affected after the silencing of ATG7, suggesting that E2 induces ATG7-independent and Ulk1/Rab9-dependent alternative autophagy. Although increasing pieces of evidence suggest that both LC3-dependent and LC3-independent autophagy contribute to mitochondrial autophagy, here we show that estrogen-regulated Rab9-dependent alternative autophagy is the predominant form of mitochondrial autophagy in the vasculature.

Although conventional autophagy is regulated by Ulk1 and PI3K complexes, alternative autophagy also requires Ulk1. In fact, the study of etoposide-treated and etoposide-untreated ATG5-deficient mouse embryonic fibroblasts in the context of Ulk1 silencing revealed reduced autophagic vacuoles, indicating that ATG5/ATG7-independent autophagy requires the Ulk1 complex.²⁶ Here, we show that the increase in the number of LAMP2 – Rab9 colocalizing signals induced by E2 was abolished by Ulk1 silencing, suggesting that E2-induced Rab9 dependent alternative autophagy requires Ulk1 in VSMCs and HUVECs. Although Ulk1 and PI3K are necessary for both conventional and alternative autophagy, alternative autophagy does not require Atg5 or LC3I to LC3II transition. Conventional and alternative autophagy are believed to be selectively activated by the phosphorylation/dephosphorylation of different serine/threonine residues in Ulk1. At least 13 Ulk1 phosphorylation sites have been identified.³⁴ Ulk1 is phosphorylated at serine 638 in the context of nutrient-sensing through AMPK, leading to the induction of conventional autophagy. Serine 758 (serine 757 in mouse) has also been reported to be involved in the regulation of conventional autophagy.³⁵ Additionally, serine 555 is also phosphorylated by AMPK.^{36,37} Importantly, a recent study showed that the phosphorylation of Ulk1 at serine 555 plays an essential role in the regulation of alternative autophagy via the interaction of Ulk1 with Rab9 in ischemic hearts.²⁵ We showed that E2 increased the phosphorylation of Ulk1 at the serine 555 site. On the other hand, the phosphorylation of serine 638 and serine 757 was not affected (data not shown). Therefore, we believe that the phosphorylation of Ulk1 at serine 555 contributes to the induction of alternative autophagy in vascular cells. Saito et al demonstrated that Rab9-dependent alternative autophagy contributed the maintenance of

mitochondrial quality in the form of mitophagy, derived from the activation of the Rip1-Ulk1-Rab9-Drp1 pathway.²⁵ In our study, Rip1, and Drp1 were not involved in the induction of Rab9-dependent autophagy by E2. We demonstrate that E2-induced SIRT1 contributed to the initiation of alternative autophagy via the activation of the AMPK/ULK1/Rab9 pathway as shown in Figures 4, and 5. We also confirmed that there was no significant difference comparing the mitochondrial contents of E2-treated cells in the presence or absence of the SIRT1 inhibitor, sirtinol, whereas the mitochondrial function was decreased by the inhibition of SIRT1 (data not shown). Because estrogen plays a crucial role in the induction of SIRT1, and estrogen receptors are not abundant in cardiomyocytes, we speculate that the differences in the induction of Rab9-dependent alternative autophagy between vascular cells and cardiomyocyte are owing to this fact.

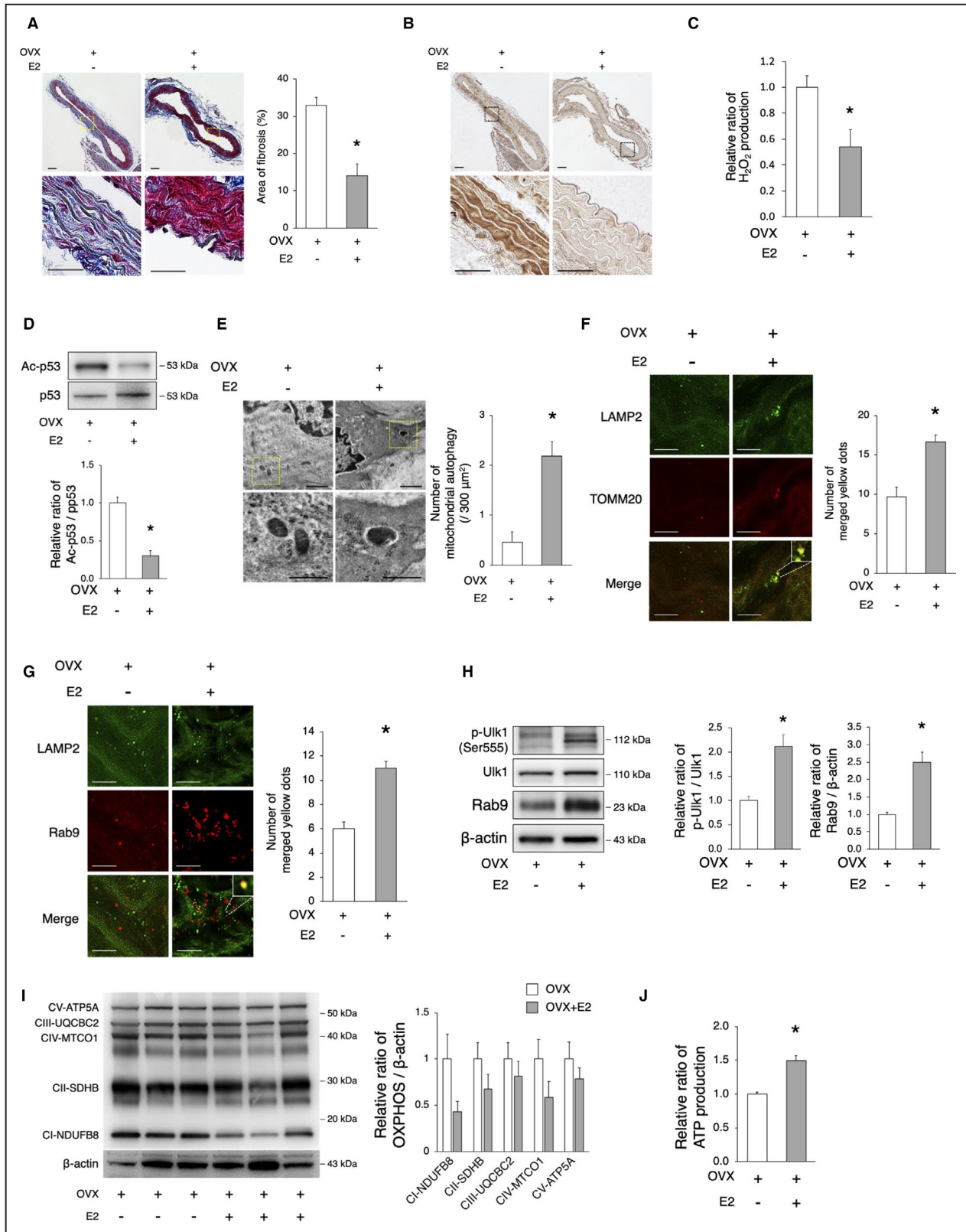
Histone deacetylases control LKB1/AMPK signaling through acetylation and de-acetylation.³⁸ Notably, SIRT1 has been reported to play a critical role in the regulation of cardiac inflammation and apoptosis through the LKB1/AMPK pathway.³⁹ In this study, we found that E2 activated LKB1 and AMPK via the phosphorylation of serine 428 and threonine 172, respectively, and this effect was abolished by sirtinol. In addition, the inhibition of AMPK by Compound C decreased the phosphorylation levels of Ulk1 at serine 555 and E2-induced Rab9, suggesting that the SIRT1/LKB1 pathway is behind the induction of alternative autophagy. These results suggest that E2 controls the activation of Ulk1 through the SIRT1/LKB1 pathway. However, the phosphorylation of AMPK at Thr172 was also reported to be involved in conventional autophagy.³⁵ Therefore, we need to further investigate how

activated AMPK controls the phosphorylation of different sites of Ulk1.

Mitochondrial dysfunction induced by metabolic stress results in vascular dysfunction, leading to the development of cardiovascular diseases.^{40,41} Mitochondrial autophagy, the selective autophagy of mitochondria, is a mechanism of mitochondrial quality control, essential for the removal of dysfunctional or damaged mitochondria. One of the well-known mechanisms to identify dysfunctional mitochondria is the PINK1 (PTEN-induced kinase 1)-Parkin-dependent mechanism.⁴² PINK1 stabilizes and accumulates in depolarized mitochondria. PINK1 activation recruits Parkin from the cytosol to the mitochondria through the phosphorylation of Parkin at serine 65.⁴³ PINK1 activation recruits LC3 receptors or adapters, including p62, NDP52, NBR1, optineurin, and Nix, and induces mitochondrial autophagy through the phosphorylation of ubiquitin and Parkin.⁴⁴ A previous study showed that mitochondrial autophagy induced by the PINK1-Parkin pathway plays a role in maintaining mitochondrial integrity and protecting vascular endothelial cells under metabolic stress conditions.⁴⁵ In addition, mitochondrial autophagy induced through PINK1 and Parkin is involved in the prevention of atherosclerosis.⁴⁶ These mechanisms enable autophagosomes through the LC3-dependent autophagy to engulf damaged mitochondria. Our study revealed that, when estrogen-free stress was applied to the mitochondria, dysfunctional mitochondria increased, but Parkin was not observed in VSMCs, indicating that mitochondrial dysfunction induced by estrogen-free stress conditions does not induce the PINK1-Parkin pathway (data not shown). A recent study also showed that Ulk1-Rab9-dependent mitochondrial autophagy was induced by

Figure 7. Estrogen rescues OVX-induced arterial senescence via the induction of mitochondrial autophagy.

OVX mice were implanted with either E2 or control pellets for 8 weeks. **A**, Assessment of aortal fibrosis in OVX and OVX+E2 mice using the Masson's trichrome staining 8 weeks after implantation. Enlarged images of the areas delineated by the dashed rectangles are shown below. The area of fibrosis was smaller in OVX+E2 mice. Scale bar, 25 μm . * $P < 0.05$ vs OVX (n=3 per group). **B**, Representative images of 4-HNE in OVX and OVX+E2 mice. Immunoreactivity of 4-HNE increased in the aorta of OVX mice compared with that of OVX+E2 mice. **C**, The relative H_2O_2 production by isolated mitochondria from the aorta of OVX and OVX+E2 mice 8 weeks after implantation was evaluated using the Amplex Red assay. H_2O_2 production was lower in OVX+E2 mice. * $P < 0.05$ vs OVX (n=3 per group). **D**, Representative immunoblots and quantitative analysis of Ac-p53 and p53 in OVX and OVX+E2 mice. The expression of Ac-p53 in OVX+E2 mice was lower than that in OVX mice. * $P < 0.05$ vs sham (n=3 per group). **E**, Electron microscopy images of the aorta from OVX and OVX+E2 mice (upper panel, scale bar, 1 μm). Enlarged images of the areas delineated by the dashed rectangles are shown below (scale bar, 500 nm). More than 900 μm^2 of the aorta of each mouse were screened in a random fashion; 3 samples per group were evaluated and the number of mitochondria engulfed by autophagosomes was counted. The number of mitochondrial autophagy was higher in OVX+E2 mice. * $P < 0.05$ vs OVX. **F**, Representative images of LAMP2 (green) and TOMM20 (red) immunohistochemistry in OVX and OVX+E2 mice. The merged yellow signals were higher in OVX+E2 mice. Scale bar, 5 μm . * $P < 0.05$ vs OVX (n=3 per group). **G**, Representative images of LAMP2 (green) and Rab9 (red) immunohistochemistry in OVX and OVX+E2 mice. The merged yellow signals were higher in OVX+E2 mice. Scale bar, 5 μm . * $P < 0.05$ vs OVX (n=3 per group). **H**, Representative immunoblots and quantitative analysis of Ulk1 and Rab9 in OVX and OVX+E2 mice. The expression of activated Ulk1 and Rab9 in OVX+E2 mice was higher than that in OVX mice. * $P < 0.05$ vs sham (n=3 per group). **I**, Representative immunoblots and quantitative analysis of total OXPHOS in OVX and OVX+E2 mice. The expression of total OXPHOS was not different between the 2 groups (n=3 per group). **J**, The relative ATP production of isolated mitochondria from the aorta of OVX and OVX+E2 mice 8 weeks after implantation was evaluated. ATP production was higher in OVX+E2 mice. * $P < 0.05$ vs OVX (n=3 per group). All data are shown as the mean \pm SEM. 4-HNE indicates 4-hydroxynonenal; E2, 17 β -estradiol; LAMP2, lysosome-associated membrane protein 2; OVX, ovariectomy; OXPHOS, oxidative phosphorylation; and TOMM20, translocase of outer mitochondrial membrane 20.



a mechanism distinct from PINK1-Parkin-dependent mitochondrial autophagy in myocardial ischemia.²⁵ Similarly, our experimental results suggested that

estrogen-induced mitochondrial autophagy in vascular cells may be PINK1-Parkin-independent. However, how the alternative autophagy machinery recognizes

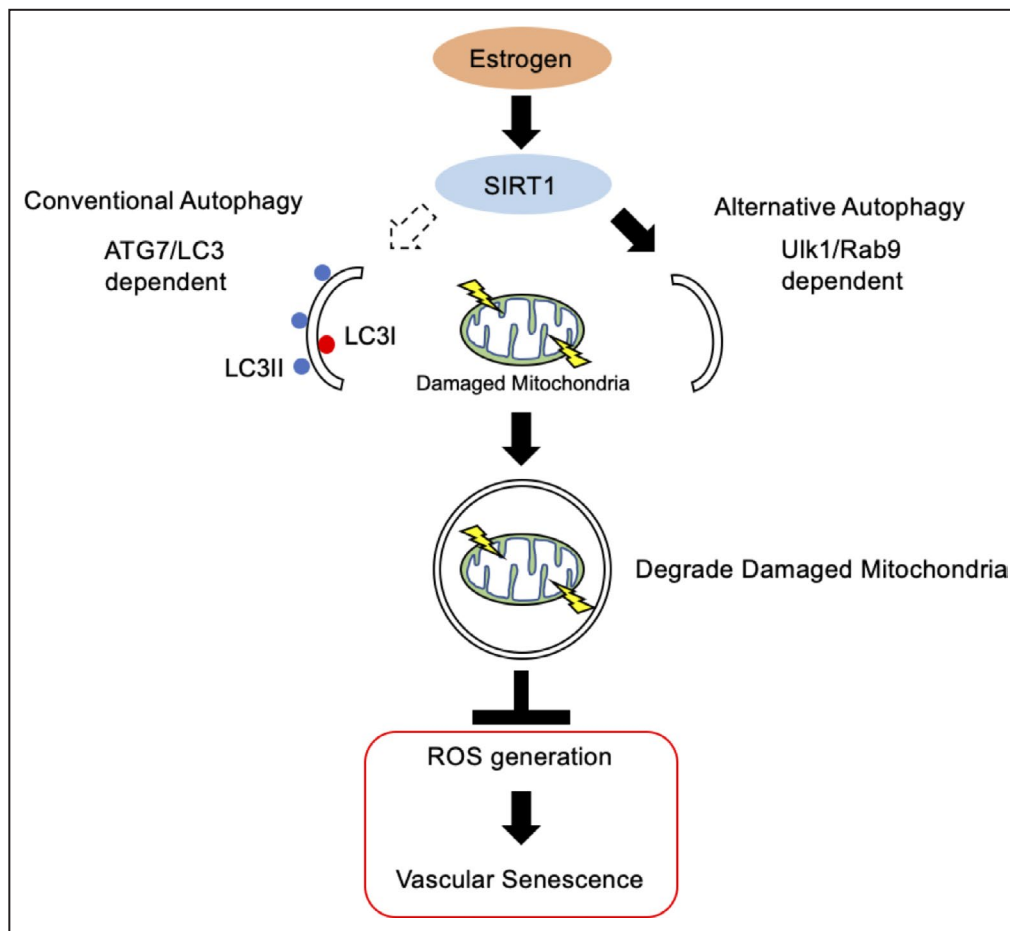


Figure 8. The proposed mechanism of the effect of estrogen on the delay of arterial senescence.

Estrogen increases mitochondrial autophagy, contributing to mitochondrial quality control and delaying cellular senescence. Rab9 dependent alternative autophagy, but not conventional autophagy, is the predominant form of E2-induced mitochondrial autophagy. The effect of E2 on the induction of Rab9 is mediated by the SIRT1/LKB1/AMPK/Ulk1 pathway. As a result, mitochondrial autophagy derived from SIRT1/LKB1/AMPK/Ulk1/Rab9-mediated alternative autophagy plays a key role in the effect of estrogen on the delay of vascular senescence. AMPK indicates adenosine monophosphate-activated protein kinase; ATG7, autophagy related 7; E2, 17 β -estradiol; LC3, light chain 3; LKB1, liver kinase B1; ROS, reactive oxygen species; and SIRT1, sirtuin 1.

damaged mitochondria in the vasculature is still unknown. We previously showed that OVX induces arterial senescence and atherosclerosis through the downregulation of SIRT1 and that the administration of estrogen prevents these alterations via SIRT1 induction.²⁴ However, up to now, no molecules downstream of SIRT1 were involved in the suppression of the development of vascular aging and atherosclerosis. Here, we found that the estrogen/SIRT1/LKB1/Ulk1/Rab9 axis plays a crucial role in the mediation of alternative autophagy, which acts as mitochondrial autophagy, removing damaged mitochondria and delaying vascular senescence (Figure 8). We believe that our finding may contribute to develop new therapeutic approach to inhibit atherosclerotic cardiovascular diseases in postmenopausal women.

Limitations

The precise mechanism behind mitochondrial autophagy induced by E2, particularly, how the Rab9-dependent alternative autophagy recognizes damaged mitochondria in a PINK1-Parkin pathway-independent manner, needs to be determined. Furthermore, in vivo experiments using a mouse specifically knocked out of phosphorylated Ulk1 at serine 555, are essential to determine whether alternative autophagy is suppressed. Moreover, arterial-specific loss of function studies (eg, Rab9 conditional knockout) in vivo were not conducted in this study, and should be performed in the future.

ARTICLE INFORMATION

Received September 26, 2020; accepted January 28, 2021.

Affiliations

From the Department of Cardiovascular Medicine and Hypertension, Graduate School of Medical and Dental Sciences, Kagoshima University, Kagoshima, Japan (Y.S., Y.I., Y.U., Y.A., M.O.); and Department of Cell Biology and Molecular Medicine, Rutgers New Jersey Medical School, Newark, NJ (J.S.).

Acknowledgments

We thank Ms Michiko Shimokawa, Ms Ayako Kuroki, and Ms Aya Yanagi for their excellent technical assistance and all of the staff members of the Institute of Laboratory Animal Science, Kagoshima University (Frontier Science Research Center) for maintaining the animals in good condition. We also thank the joint Research Laboratory, Kagoshima University Graduate School of Medical and Dental Science, for allowing the use of their facilities.

Sources of Funding

This work was supported by the Japan Society for the Promotion of Science KAKENHI (Grant No., JP16K09250).

Disclosures

None.

Supplementary Material

Supplemental Materials and Methods

Figures S1–S8

References 47–49

REFERENCES

- Sheffield-Moore M, Urban RJ. An overview of the endocrinology of skeletal muscle. *Trends Endocrinol Metab.* 2004;15:110–115. DOI: 10.1016/j.tem.2004.02.009.
- Stevenson JC. A woman's journey through the reproductive, transitional and postmenopausal periods of life: impact on cardiovascular and musculo-skeletal risk and the role of estrogen replacement. *Maturitas.* 2011;70:197–205.
- Viña J, Lloret A. Why women have more Alzheimer's disease than men: gender and mitochondrial toxicity of amyloid- β peptide. *J Alzheimer's Dis.* 2010;20:S527–S533. DOI: 10.3233/JAD-2010-100501.
- Barton M, Meyer MR, Haas E. Hormone replacement therapy and atherosclerosis in postmenopausal women: does aging limit therapeutic benefits? *Arterioscler Thromb Vasc Biol.* 2007;27:1669–1672. DOI: 10.1161/ATVBAHA.106.130260.
- Xing D, Nozell S, Chen YF, Hage F, Oparil S. Estrogen and mechanisms of vascular protection. *Arterioscler Thromb Vasc Biol.* 2009;29:289–295. DOI: 10.1161/ATVBAHA.108.182279.
- Kannel WB, Hjortland MC, McNamara PM, Gordon T. Menopause and risk of cardiovascular disease: the Framingham study. *Ann Intern Med.* 1976;85:447–452. DOI: 10.7326/0003-4819-85-4-447.
- Hodis HN, Mack WJ, Henderson VW, Shoupe D, Budoff MJ, Hwang-Levine J, Li Y, Feng M, Dustin L, Kono N, et al. Vascular effects of early versus late postmenopausal treatment with estradiol. *N Engl J Med.* 2016;374:1221–1231. DOI: 10.1056/NEJMoa1505241.
- Finkel T, Serrano M, Blasco MA. The common biology of cancer and ageing. *Nature.* 2007;448:767–774. DOI: 10.1038/nature05985.
- Denzel MS, Storm NJ, Gutschmidt A, Baddi R, Hinze Y, Jarosch E, Sommer T, Hoppe T, Antebi A. Hexosamine pathway metabolites enhance protein quality control and prolong life. *Cell.* 2014;156:1167–1178. DOI: 10.1016/j.cell.2014.01.061.
- Buchberger A, Bukau B, Sommer T. Protein quality control in the cytosol and the endoplasmic reticulum: brothers in arms. *Mol Cell.* 2010;40:238–252. DOI: 10.1016/j.molcel.2010.10.001.
- Levine B, Kroemer G. Autophagy in the pathogenesis of disease. *Cell.* 2008;132:27–42. DOI: 10.1016/j.cell.2007.12.018.
- Rubinsztein DC, Mariño G, Kroemer G. Autophagy and aging. *Cell.* 2011;146:682–695. DOI: 10.1016/j.cell.2011.07.030.
- Larocca TJ, Henson GD, Thorburn A, Sindler AL, Pierce GL, Seals DR. Translational evidence that impaired autophagy contributes to arterial ageing. *J Physiol.* 2012;590:3305–3316. DOI: 10.1113/jphysiol.2012.229690.
- LaRocca TJ, Gioscia-Ryan RA, Hearon CM, Seals DR. The autophagy enhancer spermidine reverses arterial aging. *Mech Ageing Dev.* 2013;134:314–320. DOI: 10.1016/j.mad.2013.04.004.
- Xiang J, Liu X, Ren J, Chen K, Wang HL, Miao YY, Qi MM. How does estrogen work on autophagy? *Autophagy.* 2019;15:197–211. DOI: 10.1080/15548627.2018.1520549.
- Sun N, Youle RJ, Finkel T. The mitochondrial basis of aging. *Mol Cell.* 2016;61:654–666. DOI: 10.1016/j.molcel.2016.01.028.
- Lakatta EG, Levy D. Arterial and cardiac aging: major shareholders in cardiovascular disease enterprises: part I: aging arteries: a “set up” for vascular disease. *Circulation.* 2003;107:139–146. DOI: 10.1161/01.CIR.0000048892.83521.58.
- North BJ, Sinclair DA. The intersection between aging and cardiovascular disease. *Circ Res.* 2012;110:1097–1108. DOI: 10.1161/CIRCRESAHA.111.246876.
- Youle RJ, Narendra DP. Mechanisms of mitophagy. *Nat Rev Mol Cell Biol.* 2011;12:9–14. DOI: 10.1038/nrm3028.
- Saito T, Sadoshima J. Molecular mechanisms of mitochondrial autophagy/mitophagy in the heart. *Circ Res.* 2015;116:1477–1490. DOI: 10.1161/CIRCRESAHA.116.303790.
- Wei Y, Huang J. Role of estrogen and its receptors mediated-autophagy in cell fate and human diseases. *J Steroid Biochem Mol Biol.* 2019;191:105380.–10.1016/j.jsbmb.2019.105380.
- Hofland LJ, van Koetsveld P, Koper JW, den Holder A, Lamberts SWJ. Weak estrogenic activity of phenol red in the culture medium: its role in the regulation of prolactin release in vitro. *Mol Cell Endocrinol.* 1987;54:43–50. DOI: 10.1016/0303-7207(87)90138-9.
- Węsierska-Gądek J, Schreiner T, Maurer M, Waringer A, Ranftler C. Phenol red in the culture medium strongly affects the susceptibility of human MCF-7 cells to roscovitine. *Cell Mol Biol Lett.* 2007;12:280–293. DOI: 10.2478/s11658-007-0002-5.
- Sasaki Y, Ikeda Y, Miyauchi T, Uchikado Y, Akasaki Y, Ohishi M. Estrogen-SIRT1 axis plays a pivotal role in protecting arteries against menopause-induced senescence and atherosclerosis. *J Atheroscler Thromb.* 2020;27:47–59. DOI: 10.5551/jat.47993.
- Saito T, Nah J, Oka S, Mukai R, Monden Y, Maejima Y, Ikeda Y, Sciarretta S, Liu T, Li H, et al. An alternative mitophagy pathway mediated by Rab9 protects the heart against ischemia. *J Clin Invest.* 2019;129:802–819. DOI: 10.1172/JCI122035.
- Nishida Y, Arakawa S, Fujitani K, Yamaguchi H, Mizuta T, Kanaseki T, Komatsu M, Otsu K, Tsujimoto Y, Shimizu S. Discovery of Atg5/Atg7-independent alternative macroautophagy. *Nature.* 2009;461:654–658. DOI: 10.1038/nature08455.
- Ikeda Y, Shirakabe A, Brady C, Zablocki D, Ohishi M, Sadoshima J. Molecular mechanisms mediating mitochondrial dynamics and mitophagy and their functional roles in the cardiovascular system. *J Mol Cell Cardiol.* 2015;78:116–122. DOI: 10.1016/j.yjmcc.2014.09.019.
- Kaeberlein M, McVey M, Guarente L. The SIR2/3/4 complex and SIR2 alone promote longevity in *Saccharomyces cerevisiae* by two different mechanisms. *Genes Dev.* 1999;13:2570–2580. DOI: 10.1101/gad.13.19.2570.
- Ungvari Z, Tarantini S, Donato AJ, Galvan V, Csiszar A. Mechanisms of vascular aging. *Circ Res.* 2018;123:849–867. DOI: 10.1161/CIRCRESAHA.118.311378.
- Lan F, Cacicedo JM, Ruderman N, Ido Y. SIRT1 modulation of the acetylation status, cytosolic localization, and activity of LKB1: possible role in AMP-activated protein kinase activation. *J Biol Chem.* 2008;283:27628–27635. DOI: 10.1074/jbc.M805711200.
- Kuma A, Hatano M, Matsui M, Yamamoto A, Nakaya H, Yoshimori T, Ohsumi Y, Tokuhiisa T, Mizushima N. The role of autophagy during the early neonatal starvation period. *Nature.* 2004;432:1032–1036. DOI: 10.1038/nature03029.
- Komatsu M, Waguri S, Ueno T, Iwata J, Murata S, Tanida I, Ezaki J, Mizushima N, Ohsumi Y, Uchiyama Y, et al. Impairment of starvation-induced and constitutive autophagy in Atg7-deficient mice. *J Cell Biol.* 2005;169:425–434. DOI: 10.1083/jcb.200412022.
- Shimizu S. Biological roles of alternative autophagy. *Mol Cells.* 2018;41:50–54.
- Alers S, Löffler AS, Wesselborg S, Stork B. Role of AMPK-mTOR-Ulk1/2 in the regulation of autophagy: cross talk, shortcuts, and feedbacks. *Mol Cell Biol.* 2012;32:2–11. DOI: 10.1128/MCB.06159-11.
- Shang L, Chen S, Du F, Li S, Zhao L, Wang X. Nutrient starvation elicits an acute autophagic response mediated by Ulk1 dephosphorylation and its subsequent dissociation from AMPK. *Proc Natl Acad Sci USA.* 2011;108:4788–4793. DOI: 10.1073/pnas.1100844108.
- Egan DF, Shackelford DB, Mihaylova MM, Gelino S, Kohnz Rebecca A, Mair W, Vasquez DS, Joshi A, Gwinn DM, Taylor R, et al. Phosphorylation

- of ULK1 (hATG1) by AMPK-activated protein kinase connects energy sensing to mitophagy. *Science*. 2011;331:456–461.
37. Bach M, Larance M, James DE, Ramm G. The serine/threonine kinase ULK1 is a target of multiple phosphorylation events. *Biochem J*. 2011;440:283–291. DOI: 10.1042/BJ20101894.
 38. Mihaylova MM, Shaw RJ. Metabolic reprogramming by class I and II histone deacetylases. *Trends Endocrinol Metab*. 2013;24:48–57. DOI: 10.1016/j.tem.2012.09.003.
 39. Zheng Z, Chen H, Li J, Li T, Zheng B, Zheng Y, Jin H, He Y, Gu Q, Xu N. Sirtuin 1-mediated cellular metabolic memory of high glucose via the LKB1/AMPK/ROS pathway and therapeutic effects of metformin. *Diabetes*. 2012;61:217–228. DOI: 10.2337/db11-0416.
 40. Madamanchi NR, Runge MS. Mitochondrial dysfunction in atherosclerosis. *Circ Res*. 2007;100:460–473. DOI: 10.1161/01.RES.0000258450.44413.96.
 41. Kluge MA, Fetterman JL, Vita JA. Mitochondria and endothelial function. *Circ Res*. 2013;112:1171–1188. DOI: 10.1161/CIRCRESAHA.111.300233.
 42. Narendra D, Tanaka A, Suen DF, Youle RJ. Parkin is recruited selectively to impaired mitochondria and promotes their autophagy. *J Cell Biol*. 2008;183:795–803. DOI: 10.1083/jcb.200809125.
 43. Nguyen TN, Padman BS, Lazarou M. Deciphering the molecular signals of PINK1/Parkin mitophagy. *Trends Cell Biol*. 2016;26:733–744. DOI: 10.1016/j.tcb.2016.05.008.
 44. Lazarou M, Sliter DA, Kane LA, Sarraf SA, Wang C, Burman JL, Sideris DP, Fogel AI, Youle RJ. The ubiquitin kinase PINK1 recruits autophagy receptors to induce mitophagy. *Nature*. 2015;524:309–314. DOI: 10.1038/nature14893.
 45. Wu W, Xu H, Wang Z, Mao Y, Yuan Y, Luo W, Cui Z, Cui T, Wang XL, Shen YH. PINK1-parkin-mediated mitophagy protects mitochondrial integrity and prevents metabolic stress-induced endothelial injury. *PLoS One*. 2015;10:1–14. DOI: 10.1371/journal.pone.0132499.
 46. Bravo-San Pedro JM, Kroemer G, Galluzzi L. Autophagy and mitophagy in cardiovascular disease. *Circ Res*. 2017;120:1812–1824. DOI: 10.1161/CIRCRESAHA.117.311082.
 47. Yang HJ, Kong B, Shuai W, Zhang J, Huang H. MD1 deletion exaggerates cardiomyocyte autophagy induced by heart failure with preserved ejection fraction through ROS/MAPK signalling pathway. *J Cell Mol Med*. 2020;24:9300–9312. DOI: 10.1111/jcmm.15579.
 48. Miyauchi T, Miyata M, Ikeda Y, Akasaki Y, Hamada N, Shirasawa T, Furusho Y, Tei C. Waon therapy upregulates Hsp90 and leads to angiogenesis through the AKT-endothelial nitric oxide synthase pathway in mouse hindlimb ischemia. *Circ J*. 2012;76:1712–1721. DOI: 10.1253/circj.CJ-11-0915.
 49. Ikeda Y, Shirakabe A, Maejima Y, Zhai P, Sciarretta S, Toli J, Nomura M, Mihara K, Egashira K, Ohishi M, et al. Endogenous Drp1 mediates mitochondrial autophagy and protects the heart against energy stress. *Circ Res*. 2015;116:264–278. DOI: 10.1161/CIRCRESAHA.116.303356.

Supplemental Material

Data S1.

Expanded Materials & Methods

Cell lines and culture methods

Human umbilical vein endothelial cells (HUVECs) and human aortic smooth muscle cells (SMCs) were purchased from Lonza Group Ltd. (Basel, CHE). They were cultured in endothelial growth medium (EGM-2; EGM-2 SingleQuots, Lonza) or SMC growth medium (SmGM-2; SmGM-2 SingleQuots, Lonza), as described previously.²⁴ When the cells reached 80% confluency, the culture medium was replaced with phenol red-free Dulbecco's modified Eagle's Medium (DMEM; GIBCO, Invitrogen) with 10% charcoal-stripped fetal bovine serum (FBS; Biowest) and maintained for 24 h before E2 treatment, as phenol red is known to possess estrogenic properties.^{22,23}

Cell treatment

Cells were treated with 10 nmol/L E2 in phenol red-free DMEM supplemented with 2% charcoal-stripped FBS. Control cells were exposed to the same volume of medium without E2. For the inhibition experiments, the culture medium was exchanged with DMEM containing 2% charcoal-stripped FBS and maintained for 30 min, 1 h, 3 h, 6 h, and 24 h before the addition of ICI 182780

(1 $\mu\text{mol/L}$; Sigma), sirtinol (50 $\mu\text{mol/L}$; Sigma), compound C (10 $\mu\text{mol/L}$; Sigma), or G15 (2 $\mu\text{mol/L}$; Cayman).

Animal models

All animal experiments were conducted in compliance with the protocol reviewed by the Institutional Animal Care and Use Committee and approved by the Faculty of Medicine, Kagoshima University, and followed the recommendations of the guidelines for animal experimentation at research institutes (Ministry of Education, Culture, Sports, Science and Technology, Japan and Ministry of Health, Labor and Welfare, Japan) and the guidelines for the proper conduct of animal experimentation (Science Council of Japan). 12-week-old female C57BL/6 mice or ApoE KO mice were anesthetized with a combination of 0.3 mg/kg medetomidine, 4.0 mg/kg midazolam, and 5.0 mg/kg butorphanol by intraperitoneal injection (i.p.) and subjected in a random and allocation concealment fashion to bilateral ovariectomy (OVX) or sham surgery. We used 6 to 7 animals per group in each experiments, and assigned 3 animals for immunohistochemical analysis and the other animals for immunoblot analysis. Bodyweight and food intake were measured every week after the surgical procedures as described previously.²⁴ In a different experiment, 12-week-old (Young) and 90-week-old (Old) female C57BL/6 mice were used.

Experimental procedures

The effects of E2 in OVX mice were investigated via the subcutaneous implantation of E2 pellets (0.5 mg per pellet releasing 8.3 µg/day; Innovative Research; OVX + E2), or control pellets (OVX) for 8 weeks, as previously described.²⁴ To inhibit conventional autophagy, OVX mice implanted with an E2 pellet were treated with either 3-MA (10 mg/kg) or with PBS as vehicle via i.p. injection five days per week for 2 weeks.⁴⁷

Tissue preparation and estradiol analysis

All mice were killed with an overdose of sodium pentobarbital 8 weeks after surgery, and blood samples were collected from the left ventricle, as reported previously.⁴⁸ After blood was drawn, mice were perfused with phosphate-buffer saline (pH 7.4), and the vessels were harvested for use in the following experiments. The ascending aortas were immediately fixed with 4 % paraformaldehyde phosphate buffer solution for Masson's Trichrome staining and immunohistochemical analysis. For electron microscopy analysis, the removed vessels were immediately placed into electron microscopy fixative. For immunoblot analysis, the isolated vessels were rinsed in phosphate buffered saline and stored at -80°C until use. For mitochondrial isolation, aorta samples from the ascending artery to the bifurcation of the common iliac artery were

harvested and immediately used in the experiment on ice. Serum was obtained by centrifugation of blood for 10 min at 850 g and 4°C and stored at -80°C. The concentration of 17β estradiol was measured enzymatically using a commercially available kit (VioVision).

Histological analysis

Histological analysis was performed as described elsewhere.⁴⁹ In brief, mice aortas were fixed with 4 % paraformaldehyde phosphate buffer solution, embedded in paraffin, and sectioned into 4 μm tissue sections. Interstitial fibrosis was evaluated using the Masson's trichrome staining.

Immunoblot analysis

Cell lysates from in vitro and in vivo samples were processed and used for immunoblot analysis using a NUPAGE Electrophoresis System (Invitrogen), as reported previously.⁴⁷ The primary antibodies used were as follows: p53 (Cell Signaling Technology, 9282, and Santa Cruz, sc99), , Acetyl-p53 (Cell Signaling Technology, 2570), AMPKα (Cell Signaling Technology, 2532), phospho-AMPKα (Th172; Cell Signaling Technology, 2535), LKB1 (Cell Signaling Technology, 3050), phospho-LKB1(Ser428; Cell Signaling Technology, 3482), Atg7 (Cell Signaling Technology, 2631), SIRT1 (Merck Millipore, 07-131), Ulk1 (Abcam, ab128859), phospho-Ulk1(Ser555; Merck Millipore,

ABC 124 and Cell Signaling Technology, 5869), p21 (Santa Cruz, sc6246), p16 (Santa Cruz, sc1207), PAI-1 (Santa Cruz, sc8979), p62 (SQSTM1; MBL, PM045), LC3 (MBL, M186-3), Rab9 (Sigma, R5404), Drp1 (DLP1; BD Biosciences, 611112), phosphor-Drp1 (Ser616; Cell Signaling Technology, 4494), phosphor-Drp1 (Ser637; Abcam, ab193216), PGC1- α (Santa Cruz, sc518025), Mfn1 (Abcam, ab57602), Mfn2 (Sigma, M6319), OPA1 (BD Biosciences, 612606), Rip1 (Cell Signaling Technology, 3493S), total OXPHOS (Abcam, ab110413), β -actin (Santa Cruz, sc47778), and α -tubulin (Sigma, T9026). Either horseradish peroxidase-conjugated goat anti-rabbit antibody (Bio-Rad, 1706515) or goat anti-mouse antibody (Santa Cruz, 516102) was then added. Densitometric analyses were performed using the ECL prime system (GE Healthcare UK Ltd., Little Chalfont, UK).

Immunohistochemistry

Immunohistochemistry staining of the tissue sections and cultured cells was performed, as described previously.⁴⁷ Briefly, tissue sections and cultured cells were stained with anti-Rab9 mouse monoclonal antibody (1:100; Abcam, ab2810), anti-LAMP2 rabbit polyclonal antibody (1:100; Sigma, L0668), anti-TOMM20 rabbit monoclonal antibody (1:100; Abcam, ab186734), anti-LC3B rabbit polyclonal antibody (1:100; Abcam, ab51520), Alexa Fluor 488-conjugated goat anti-

rabbit IgG (1:100; Abcam, ab150081), and Alexa Fluor 594-conjugated goat anti-mouse IgG (1:100; Abcam, ab150120). Analyses were performed using a confocal microscope (Zeiss, LSM700). The cells of each group were randomly selected from 3 independent experiments and the merged signals (yellow) were counted. Tissue sections were also incubated with primary anti-4 hydroxynonenal (4-HNE) antibody (1:50; Abcam, ab46545), then treated with an amino acid polymer conjugated to anti-rabbit IgG Fab' labeled with horseradish peroxidase (Histofine Simple Stain Mouse MAX-PO, Nichirei) and then developed using the Histofine Simple Stain DAB solution (Nichirei). Analyses were performed using fluorescence microscopy (Keyence, BZ-X710). The number of merged yellow signals were counted in the aortic sections of mice for each sample.

Senescence-associated β -galactosidase staining

Senescence-associated β -galactosidase (SA- β gal) activity was measured using a SA- β gal staining kit (Cell Signaling Technology), according to the manufacturer's protocol. SA- β gal-positive cells were counted using a microscope (Keyence, BZ-X710), as reported previously.²⁴ Briefly, more than 200 cells in, at least 5 random fields were counted to determine the percentage of SA- β gal-positive cells.

Transmission electron microscopy analysis

The harvested vessels of mice and cultured HUVECs and VSMCs were fixed in 0.2 mol/L sodium cacodylate-buffered (pH 7.4), 5 % glutaraldehyde solution for 2 h, and then rinsed (2 × 10 min) in 0.1 mol/L sodium cacodylate-buffered (pH 7.4) 7.5 % saccharose and post-fixed in 2 % OsO₄ solution for 2 h. After dehydration in an ethanol gradient (50 % ethanol for 5 min, 70 % ethanol for 5 min, 90 % ethanol for 10 min, and 100 % ethanol for 3 × 10 min), samples were embedded in EPON812. Ultrathin sections were stained with uranyl acetate and lead citrate. Sections were examined using a HITACHI H-7650 transmission electron microscope (HITACHI, Tokyo, Japan) at 80 kV.

Mitochondrial isolation

The mitochondrial fraction of HUVECs and VSMCs was purified using a mitochondrial isolation kit (Thermo Scientific), according to the manufacturer's instructions. The mitochondrial fraction of the isolated mice aorta was purified using a different mitochondrial isolation kit (MITOISO1; Sigma), according to the manufacturer's instructions.

Evaluation of mitochondrial superoxide production

Intra-mitochondrial superoxide production was measured using the MitoSox Red mitochondrial superoxide indicator for live-cell imaging (Invitrogen), according to the manufacturer's protocol. Fluorescence was observed under a microscope (Keyence, BZ-X710) equipped with an 20× Plan Apochromat 20×/0.8 N.A objective.

H₂O₂ measurement

H₂O₂ production was measured using the Amplex Red H₂O₂ assay kit (Molecular Probes; Invitrogen), according to the manufacturer's instructions.

ATP production

ATP production was measured with the ATP Bioluminescent Assay kit (Sigma). Briefly, mitochondria (20 µg) were incubated in the ATP assay mix and MSH buffer containing 625 µmol/L ADP and substrate (10 mmol/L pyruvate and 10 mmol/L malate).

Mitochondrial membrane potential evaluation

The state and integrity of the mitochondrial membrane potential was visualized via the staining of cultured cells with 5,5',6,6'-tetrachloro-1,1',3,3'-tetramethylbenzimidazolocarboyanine iodide (JC-

1) and tetramethylrhodamine ethyl ester (TMRE), using the MitoPT®JC-1 and MitoPT®TMRE (ImmunoChemistry Technologies) kits, respectively, according to the manufacturer's instructions.

The number of green fluorescent cells was determined within at least 100 cells, counted in no less than 3 random fields; the percentage of green-fluorescent cells was then calculated.

Mitotracker staining

Mitochondria were stained with MitoTracker Red FM (Invitrogen) according to the manufacturer's instructions. Fluorescence images of live cells were obtained using the LSM700 confocal laser scanning microscope (Zeiss, LSM700). To quantify mitochondrial morphology, a cell was judged to have fragmented mitochondria if > 50% of the mitochondria visible in the cell were punctate or circular. We randomly selected > 80 cells in independent 3 experiments and calculated the percentage of cells with fragmented mitochondria.

Short interfering RNA transfection

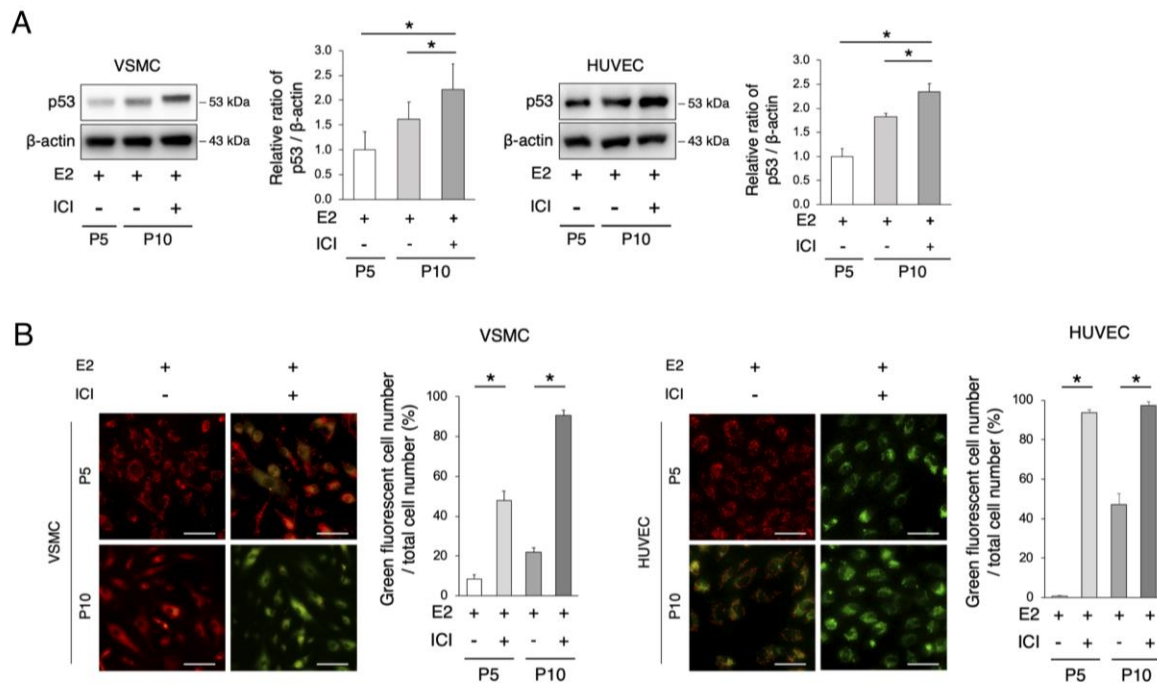
For Rab9 RNA knockdown, cells were transfected with Rab9 or control siRNA (Santa Cruz, sc-44065, sc-37007) using the siRNA Transfection Reagent (Santa Cruz, sc-29528), according to the manufacturer's instruction. For ATG7 RNA knockdown, cells were transfected with the

corresponding siRNA (Thermo Fisher Scientific) using the Lipofectamine RNAiMAX transfection reagent (13778150; Invitrogen), according to the manufacturer's protocol. Immunoblots of lysates were performed to confirm the knockdown efficiency.

Statistical analysis

Data are expressed as the mean \pm standard error of the mean (SEM). The student's *t*-test was used to determine the statistical significance of differences between two groups. For data sets with a skewed distribution or smaller sample size ($n = 3$ to 5 per group), the nonparametric statistical analysis was performed using the Wilcoxon rank sum test. Exceptions were the data in Figure 1A, 2E, 2F, and Figure S1B that were analyzed by two-way analysis of variance. Analyses were performed by JMP Pro 15 (SAS Institute, Cary, NC, USA). *P* values <0.05 were considered significant.

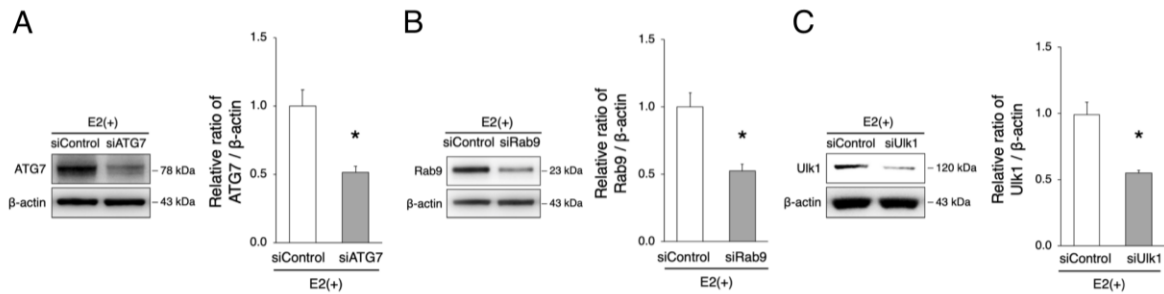
Figure S1. Estrogen delays cell aging via the maintenance of the mitochondrial function.



A, Immunoblots, and quantitative analysis results of p53 are shown. The protein expression of p53 was higher in E2-treated cells collected after 10 passages than those collected after 5 passages. The administration of ICI attenuated the E2-mediated delay of p53 expression in E2-treated cells collected after 10 passages. $*P < 0.05$ vs. E2(-) ($n = 6$ per group). **B**, The mitochondrial membrane potential was evaluated using JC-1. Red indicates mitochondria in which the membrane potential is maintained, whereas green indicates depolarized mitochondria. The quantification of HUVECs and VSMCs with depolarized mitochondria is shown. Scale bar, 50 μm . $*P < 0.05$ vs E2 (HUVECs, $n = 5$ per group; VSMCs, $n = 5$ per group). Statistical analysis was performed using 2-way analysis of variance. All data are shown as the mean \pm SEM. E2 indicates 17 β -estradiol; HUVECs, human umbilical vein endothelial cells; VSMCs, vascular smooth muscle cells.

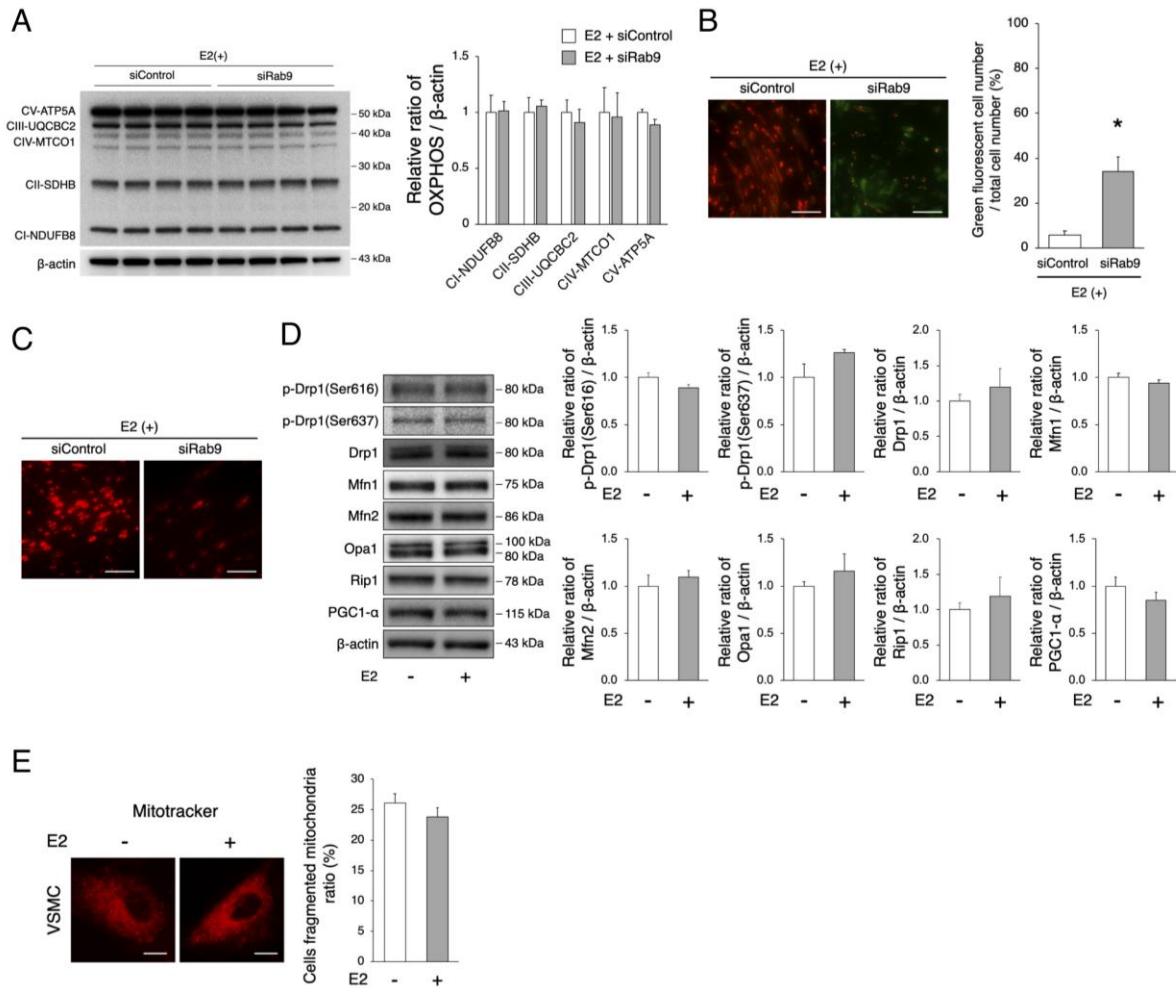
Figure S2. Autophagy-related factors were knockdown via siRNA-transfection in E2 treated

VSMCs.



A, Representative immunoblots of ATG7 are shown in E2-treated VSMCs transfected with siATG7 or siControl. * $P < 0.05$ vs. siControl (n = 3 per group). **B**, Representative immunoblots of Rab9 are shown in E2-treated VSMCs transfected with siRab9 or siControl. * $P < 0.05$ vs. siControl (n = 3 per group). **C**, Representative immunoblots of Ulk1 are shown in E2-treated VSMCs transfected with siUlk1 or siControl. * $P < 0.05$ vs siControl (n = 3 per group). All data are shown as the mean \pm SEM. E2 indicates 17 β -estradiol; VSMCs, vascular smooth muscle cells.

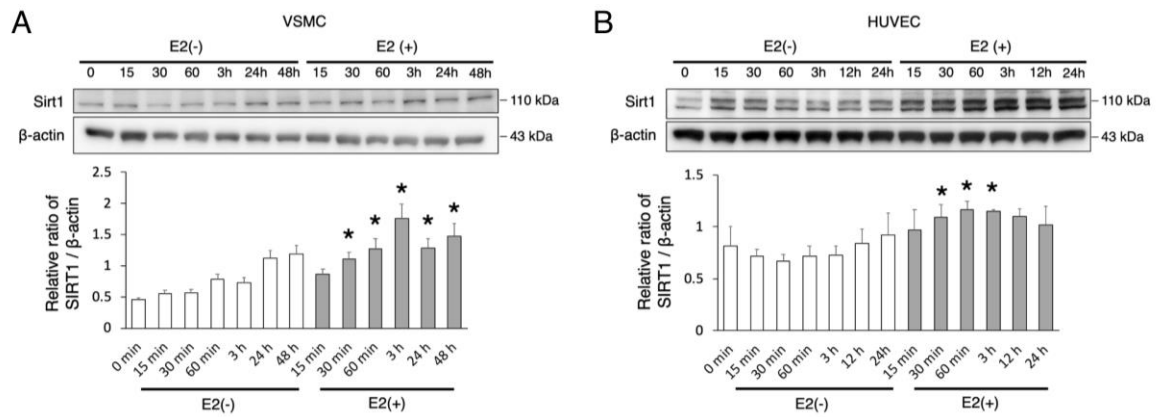
Figure S3. E2 is not involved in mitochondrial dynamics and maintains the mitochondrial function via Rab9 dependent alternative autophagy.



A, Representative immunoblots and quantitative analysis of total OXPHOS in E2-treated VSMCs transfected with siRab9 or siControl. The expression of total OXPHOS was not different between the two groups ($n = 3$ per group). **B**, The mitochondrial membrane potential was evaluated using JC-1. Red indicates mitochondria in which the membrane potential is maintained, whereas green indicates depolarized mitochondria. The quantification of VSMCs with depolarized mitochondria is shown. Scale bar, 50 μ m. * $P < 0.01$ vs E2 (VSMCs, $n = 3$ per group). **C**, TMRE staining for the assessment of the mitochondrial membrane potential. Red indicates polarized mitochondria in

which the membrane potential is maintained. Scale bar, 50 μm . **D**, Representative immunoblots and quantitative analysis results of p-Drp1 (Ser616), p-Drp1 (Ser637), Drp1, Mfn1, Mfn2, Opa1, Rip1, and PGC-1 α in VSMCs with or without E2 treatment are shown. Protein expression was not different between the two groups (n = 4 per group). **E**, Mitotracker Red was added into the medium to stain mitochondria in VSMCs with or without E2. The ratio of cells with fragmented mitochondria was not different between the two groups (n = 3 per group). Scale bar, 10 μm . All data are shown as the mean \pm SEM. E2 indicates 17 β -estradiol; OXPHOS, oxidative phosphorylation; VSMCs, vascular smooth muscle cells.

Figure S4. E2 upregulates SIRT1 in HUVECs and VSMCs.



A, Representative immunoblots and quantitative analysis of SIRT1 in VSMC with or without E2

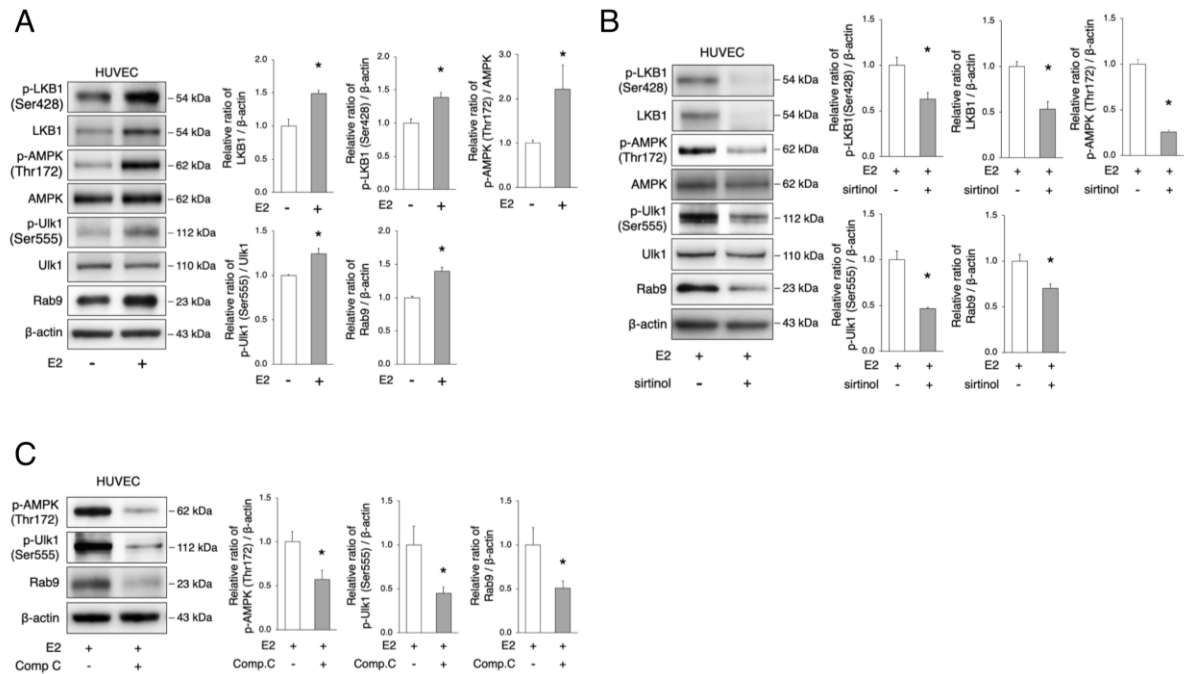
treatment for 15 min, 30 min, 1 h, 3 h, 6 h, 24 h, and 48 h. * $P < 0.05$ vs E2(-) (n = 3 per group). **B**,

Representative immunoblots and quantitative analysis of SIRT1 in HUVEC with or without E2

treatment for 15 min, 30 min, 1 h, 3 h, 12 h, and 24 h. * $P < 0.05$ vs E2(-) (n = 4 per group).

E2 indicates 17 β -estradiol; HUVECs, human umbilical vein endothelial cells; VSMCs, vascular smooth muscle cells.

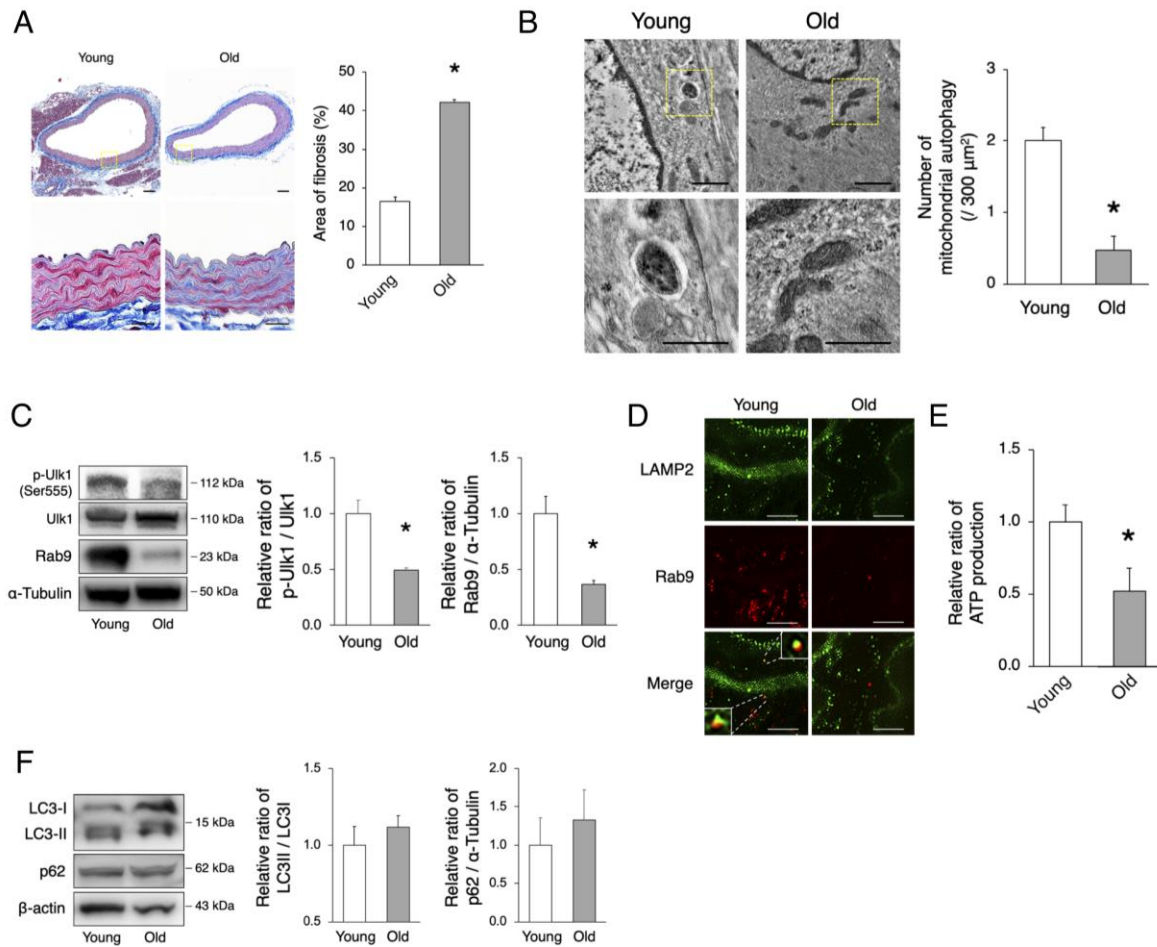
Figure S5. The SIRT1/LKB1/AMPK/UIK1 axis is involved in the induction of alternative autophagy in HUVECs.



A, Representative immunoblots and quantitative analysis of LKB1, AMPK, UIk1, and Rab9 in HUVECs with or without E2 treatment. E2 treatment activated LKB1, AMPK, UIk1, and Rab9. $*P < 0.05$ vs E2(-) (n = 3 per group). **B**, Representative immunoblots and quantitative analysis of LKB1, AMPK, UIk1, and Rab9 in E2-treated HUVECs with or without sirtinol. The administration of sirtinol attenuated the activation of LKB1, AMPK, UIk1, and Rab9 by E2. $*P < 0.05$ vs E2(+) (n = 3, 4 per group). **C**, Representative immunoblots and quantitative analysis of AMPK, UIk1, and Rab9 in E2-treated HUVECs with or without Compound C. The administration of Compound C attenuated the activation of AMPK, UIk1, and Rab9 by E2. $*P < 0.05$ vs. E2(+) (n = 4 per group).

All data are shown as the mean \pm SEM. HUVECs indicate human umbilical vein endothelial cells; E2, 17 β -estradiol.

Figure S6. Old C57BL/6 mice show signals of arterial senescence.



A, Assessment of aortic fibrosis in Young and Old mice using the Masson's trichrome staining.

Enlarged images of the areas delineated by the dashed rectangles are shown below. The area of fibrosis was greater in Old mice. Scale bar, 25 μm . * $P < 0.05$ vs. Sham ($n = 3$ per group). **B**,

Electron microscopy images of the aortas from Young and Old mice (upper panel, scale bar, 1 μm).

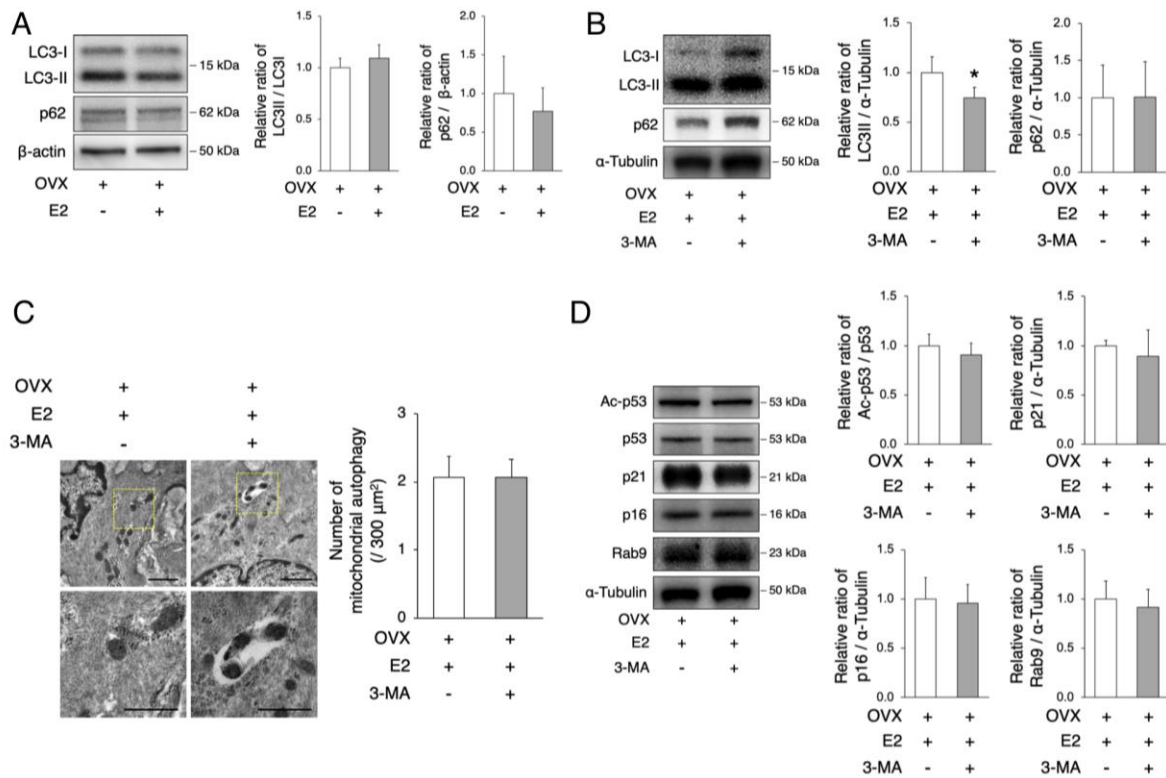
Enlarged images of the areas delineated by the dashed rectangles are shown below (scale bar,

500 nm). The aorta of each mice was randomly selected (more 1000 μm^2) in 3 samples per

group and the number of mitochondria engulfed by autophagosomes was counted. The

number of mitochondrial autophagy was lower in Old mice. $*P < 0.05$ vs. Young. **C**, Representative immunoblots and quantitative analysis of Ulk1 and Rab9 in Young and Old mice. The expression of activated Ulk1 and Rab9 in Old mice was lower than that in Young mice. $*P < 0.05$ vs. Young (n = 4 per group). **D**, Representative images of LAMP2 (green) and Rab9 (red) immunohistochemistry of the aorta in Young and Old mice. The number of Rab9 - LAMP2 co-localizing signals was lower in Old mice. **E**, Relative ATP production by isolated mitochondria from the aorta of Young and Old mice. ATP production was lower in Old versus Young mice. $*P < 0.05$ vs. Young (n = 3 per group). **F**, Representative immunoblots and quantitative analysis of LC3 and p62 in Young and Old mice. The expression of both LC3 and p62 was not different between the two groups (n = 4 per group). All data are shown as the mean \pm SEM. LAMP2 indicates lysosome-associated membrane protein 2.

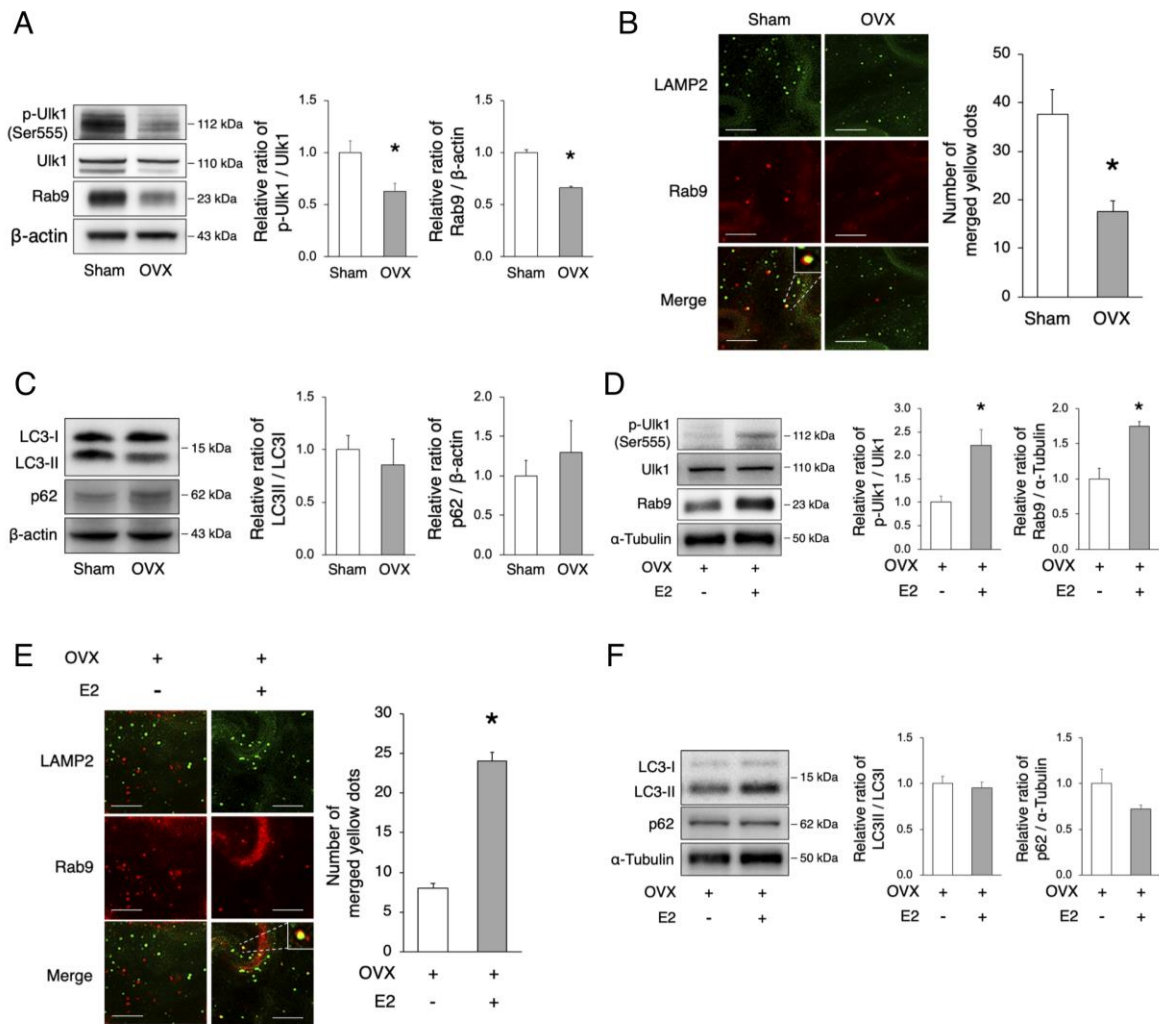
Figure S7. Effect of E2 supplementation in OVX mice.



A, OVX mice were implanted with either E2 or control pellets for 8 weeks. Representative immunoblots and quantitative analysis of LC3 and p62 in OVX and OVX + E2 mice. The expression of both LC3 and p62 was not different between the two groups (n = 3 per group). **B-D**, OVX mice were implanted with an E2 pellet were treated with or without 3-MA. **B**, Representative immunoblots and quantitative analysis of LC3 and p62 in OVX + E2 mice with or without 3-MA. The administration of 3-MA decreased the LC3II levels in OVX + E2 mice. * $P < 0.05$ vs. OVX + E2 (n = 5 per group). **C**, Representative immunoblots and quantitative analysis of Ac-p53, p21, p16, and Rab9 in OVX + E2 mice with or without 3-MA. The expression of Ac-p53, p21, p16, and Rab9

was not significantly different between the two groups (n = 5 per group). **D**, Electron microscopy images of the aorta from OVX + E2 and OVX + E2 mice treated with 3-MA (upper panel, scale bar, 1 μ m). Enlarged images of the areas delineated by the dashed rectangles are shown below (scale bar, 500 nm). The aorta of each mice was randomly selected (more 1000 μ m²) in 3 samples per group and the number of mitochondria engulfed by autophagosomes was counted. The number of mitochondrial autophagy was not different between the two groups. All data are shown as the mean \pm SEM. E2 indicates 17 β -estradiol; OVX, ovariectomy; 3-MA, 3-Methyladenine.

Figure S8. Mitochondrial autophagy in ApoE KO mice treated with E2.



A-C, Apolipoprotein E knockout (ApoE KO) mice were subjected to OVX or sham surgery. **A**, Representative immunoblots and quantitative analysis of Ulk1, and Rab9 in Sham-operated and OVX mice. The expression of activated Ulk1 and Rab9 in Sham mice was higher than that in OVX mice. * $P < 0.05$ vs. Sham ($n = 3$ per group). **B**, Representative images of LAMP2 (green) and Rab9 (red) immunohistochemistry of the aorta in Sham-operated and OVX mice. The number of yellow signals was lower in OVX mice. Scale bar, 5 μ m. * $P < 0.05$ vs. Sham ($n = 3$ per group). **C**,

Representative immunoblots and quantitative analysis of LC3 and p62 in Sham-operated and OVX mice. The expression of both LC3 and p62 was not different between the two groups (n = 3 per group). **D-E**, ApoE KO OVX mice were implanted with either E2 or control pellets for 8 weeks. **D**, Representative immunoblots and quantitative analysis of Ulk1 and Rab9 in OVX and OVX + E2 mice. The expression of activated Ulk1 and Rab9 in OVX + E2 mice was higher than that in OVX mice. **P* < 0.05 vs. Sham (n = 4 per group). **E**, Representative images of LAMP2 (green) and Rab9 (red) immunohistochemistry in OVX and OVX + E2 mice. The merged yellow signals were higher in OVX + E2 mice. Scale bar, 5 μ m. **P* < 0.05 vs OVX (n = 3 per group). **F**, Representative immunoblots and quantitative analysis of LC3 and p62 in OVX and OVX + E2 mice. The expression of both LC3 and p62 was not different between the two groups (n = 4 per group). All data are shown as the mean \pm SEM. ApoE KO indicates Apolipoprotein E knockout; E2, 17 β -estradiol; OVX, ovariectomy; LAMP2, lysosome-associated membrane protein 2.